Study of Salt Neutrino Detector (SND)

Masami Chiba, Toshio Kamijo[1], Miho Kawaki, Athar Husain,
Masahide Inuzuka, Maho Ikeda, Osamu Yasuda

Department of Physics, Tokyo Metropolitan University
[1]Department of Electrical Engineeing, Tokyo Metropolitan University
1-1 Minami-Ohsawa Hachioji-shi, Tokyo, 192-0397, Japan
<chiba-masami@c.metro-u.ac.jp>, FAX:+81-426-77-2483

Abstract

Rock salt is studied as a radiowave transmission medium in a ultra high energy (UHE) cosmic neutrino detector. The radiowave would be generated by Askar'yan effect (negative excess charges in the electromagnetic shower with coherent Chrenkov radiation) in the UHE neutrino interaction in the rock salt. Some rock salt mines are investigated whether it has a possibility as a SND site or not. The samples of the rock salts are gathered to measure the absorption length. As a tentative result, the absorption length of the radiowave is obtained around 400m at 1 GHz.

Presented by Masami Chiba at:

RADHEP2000
First International Workshop on Radio Detection of High-Energy Particles
UCLA Faculty Center, University California, Los Angeles
November 16-18, 2000

1. Introduction

Several cosmologically distant astrophysical systems could produce ultra-high-energy (UHE) cosmic neutrinos [1] over the energy of 10^{15} eV or 10^{6} GeV (PeV) whose flux probably exceeds that of the atmospheric neutrino [2]. In spite of the very low flux, we could detect extraterrestial neutrinos coming from far distance without atmospheric neutrino background. UHE neutinos are produced by astrophysical sources in cosmological distance such as Quasars (AGNs) and GRBs. They follow from the production and decay of related unstable hadrons, pions, kaons, and charmed mesons. These unstable hadrons could be produced when the accelerated protons interact with the ambient photon or protons present in the environment. The electron and muon neutrinos are mainly produced in the decay chain of charged pions whereas the tau neutrinos are mainly produced in the decay chain of charmed mesons in the same collisions at a suppressed level.

The maximum energy of cosmic rays (protons or nuclei) observed exceeds 10^{20} eV[3]. The energy is over the allowed energy for cosmic rays traveled from the extra galaxy over 50 Mpc which loses its energy in scattering processes against 3K cosmic background radiation. (GZK cutoff) [4]. It is one of the center of attention in astrophysics and high energy physics [5]. On the other hand neutrino scarcely interacts with the 3K cosmic background radiation, then it can travel long distance without losing the energy. In order to detect the UHE neutrinos, we need huge mass of the detector at least 10^{9} tons since the interaction rate is low (weak interaction) and the flux of UHE neutrinos is very low. For such a huge detector we could not give any treatment on it e.g. purification of the medium etc., then we should use it as it is naturally existed.

[Fig. 1]

The aim of the ultra-high-energy-neutrino detection is to study;

(1)ultra high energy neutrino interaction which is not afforded by artificial neutrino beam generated by an accelerator,

(2)neutrino mass problem through neutrino oscillation effect due to the long flight distances,

(3)ultra high energy accelerating mechanism of protons existing in the universe.

The interaction cross section of UHE neutrino increases but still it is not so large compared with the other interactions [6]. Although due to the increase, the number of upward neutrino is suppressed due to the absorption by the earth.

[Fig. 2]

A moderate expected event rate over PeV neutrinos is 10/year by 1km x 1km x 1km of $2x10^9$ tons of rock salt from Active Galactic Nuclei (AGN) or Quasar (QSO) and Gamma Ray Burst (GRB) by Athar Fusain et al. [7].

[Fig. 3]

The mass of the detector required to measure the UHE neutrinos should be compared with the existing large neutrino detector, Super Kamiokande (S-K), which consists of $5x10^4$ tons of pure water [8]. It is $4x10^4$ times large compared with S-K. They detects visible light generated by Cherenkov effect in the pure water. The transparency (absorption length) in a pure water is 100m at most. On the contrary, rock salt is one of the most transparent material for radiowave. The transparency of elctromagnetic wave in the frequency range under 1GHz is expected to be larger than or comparable to 1km. It means the moderate number of radiowave sensors could detect the neutrino interaction in the massive rock salt. Although if water is present in the rock salt, the transparency reduces much.

2. Coherent Cherenkov radiation

Detection of coherent Cherenkov radiation from the excess negative charges of an electron-photon shower in a dense material was proposed by G.A.Askar'yan[9]. In the range of wavelengths greater than the dimensions of the excess electron cluster, the intensity of the radiation is proportional to the squre of the total excess electron track length. The density of the medium determines the dimensions of the localized region of shower particles and the range of wavelengths in which the radiation is coherence. The small attenuation of the radio waves in rock salt, marble, granite, etc. underground is preferable. Also the absorption of radio waves in the ground of the moon should be small to use such an aim.

The presence of the excess charge in a shower may emit Cherenkov and bremsstrahlung radiation in an uniform medium. But the bremsstrahlung radiation is suppressed by LPM effect [10] and dielectric material effect [11] in the radiowave range. By the uncertainty principle the coherent formation zone extends to the longitudinal direction due to the small longitudinal momentum transfer. In the process of Coulomb multiple scattering of electrons, radio emission gets destructive interference effect. Even for 2.5MeV electrons, emission of radiowave under ~800GHz is suppressed. Stronger suppression in the emission frequency comes from deielectric material effect. Forward Compton scattering amplitude changes in phase giving destructive interference in the radio emission. For 2.5MeV electrons, emission of photons under ~150eV is suppressed. Then practically only Cherenkov radiation should be considered in a uniform medium.

Wavelength of radiowave at 1GHz and visible light at 1PHz (1×10^{15} Hz) is compared;

$$\text{Wavelength} \sim 1\ \text{GHz}\ (0.3\text{m}) \ /\ 1\text{PHz}\ (0.3\mu\text{m}) = 10^{6}.$$

Emission power of Cherenkov radiation is expressed by Frank-Tamm formula when charge ze travelling a pathlength l in a medium of refractive index n;

$$dW/(d\nu) = (2\pi h\alpha/c)z^2\nu[1 - (\beta n)^{-2}]l.$$

Radiation power at the frequency ν of 1 GHz and 1 PHz is compared;

$$dW/(d\nu) \sim 1\ \text{GHz}\ (4.1 \times 10^{-6}\ \text{eV}) \ /\ 1\ \text{PHz}\ (4.1\text{eV}) = 10^{-6}.$$

If we take into the bandwidth the detected power becomes hopelessly low 10^{-12}. to detect the radiowave. visible wavelength is much shorter than the shower size, then the radiation power is proportional to the shower energy:

$$W_{\text{visible}} \sim N\langle l\rangle,$$

where N is the number of charged particles with the average tracklength of $\langle l\rangle$. On the contrary if the wavelength is larger than the shower size, radiated wave from each excess negative charge track becomes constructively coherent with the same phase. Then the radiation power increases with the assistance of the coherent effect to a detectable level and is prortional to the squre of the shower energy;

$$W_{\text{radiowave}} \sim (\Delta q \times N)^2\langle l\rangle,$$

where Δq is a ratio of negative excess charges to the whole charges;

$$\Delta q = [N(e^-) - N(e^+)]/[N(e^-) + N(e^+)].$$

The possibility of using ice as the medium of the neutrino detector to propagate the radiowave is considered [12]. The excess electrons of the electromagnetic shower and coherent Cherenkov radiation by them are studied in detail in the case of ice [13]. The radiation power was calculated without absorption in the ice;

$$W \sim 5 \times 10^{-14}[E/1\text{TeV}]^2[\nu_{\text{max}}/1\text{GHz}]^2\ \text{erg} \sim 5 \times 10^{-15}\text{J}.$$

where we assume E = 1PeV, ν_{max} = 1 GHz.

They estimated the threshold energy E_{th} for the electromagnetic shower as a function of distance to the obsevation. At the distance of R (km), the detectable threshold energy with a reciever noise of 300K thermal equivalent with the band-width of 1GHz becomes;

$$R\ (\text{km}) \sim E_{\text{th}}\ (\text{PeV})/4.$$

[Fig. 4]

The excess electrons, Δq is 15% of the total tracklength of charged particles in ice. They are caused by the interaction of photons, positrons and electrons in the shower with the atomic electrons in the medium and generated by the Compton (~60%) and Bhabha scattering (~30%), and positron annihilation in flight (~10%). Although, Moller scattering decreases the excess charge (~-5%) due to the energy loss by the collision. Radio Ice Cherenkov Experiment (RICE) in Antarctic ice is being executed successfully and gave a neutrino flux limit [14]. Recently, Radio-frequency measurements of coherent transition and Cherenkov radiation is done using a 15.2 MeV pulsed electron beam at the Argonne Wakefield accelerator. They detected coherent radiation which is attributed both to transition and possibly Cherenkov radiation [15]. The coherent radiation was confirmed that the radiation strength was proportional to the squre of the number of electrons in a single puse.

[Fig. 5]

2-1. Comparison with optical Cherenkov radiation

Detection of optical Chrenkov radiation is the well estabish method using water (IMB, S-K, DUMAND, NESTOR, Lake Baikal, ANTARES, etc.) and ice (AMANDA, ICECUBE) [14] as the radiator. They could detect Cherenkov radiation emitted by high energy charged particles faster than the velocity of light in the medium. The detection of the light is done well developed photomultiplier tubes which could detect even one photoelectron converted at the photocathode from optical photon. The conversion efficiency , quantum efficiency, is over 20% in the optical wavelength region. Then only one charged particles passing in the detection region could be detected. Moreover muons could be detected even if a muon passed the detector region which was produced in muon neutrino charged current interactions at a far distance from the detector region. As a result it could provide a large mass of neutrino reaction region although the initial energy is not determined so definetely due to being insensitive to the energy loss between the interaction point to the detector region.

Meanwhile radio Cherenkov detection method could not detect single muon, and could not utilize the long range of high energy muons. But it utilizes special charactors that the radiation power is proportional to the squre of the shower energy due to the coherence effect among radio Cherenkov radiation from the excess electrons in the shower. And the attenuation length of radiowave is longer than optical light in the medium. Consequently, the radio sensors could be set sparsely in a huge medium. Then the huge mass could be used for detection of neutrino interaction inside the medium. The neutrino flavours of electron and tau could be detected with the energy information. Although for a muon generated from a charged current

interaction of a muon neutrino, it could not be registered after it escaped from the shower region.

2-2. Consideration on the medium density

We compare density, radiation length, refractive index, Chrenkov angle and Cherenkov threshold kinetic energy of electrons for air, ice and rock salt in table 1.

Table 1. Comparison between air, ice and rock salt in density, radiation length X_0, refractive index, Chrenkov angle θ_c and Cherenkov threshold kinetic energy for electrons Tth.

	Density (g/cm3)	X_0 (cm)	Refractive Index	θ_c (deg)	Tth (keV)
Air (STP)	0.0012	30420	1.000293	1.387	2060407
Ice	0.924	39	1.78	55.8	107
Rock salt	2.22	13	2.43	65.7	50

The density of air is 1/833 times less than rock salt and the radiation length is 2340 times larger than that even on the earth surface. Then the shower length and the diameter is much larger than ice and rock salt. The detection is not easy for such an extended air shower. In addition Cherenkov or fluorescent light detection in air shower depend on weather condition severely as well as the Sun and the Moon light. Direct particle detection of the shower by the particle detector set on the surface is not affected by such the conditions but detection of horizontal air showers are difficult. Underground detectors are neither depend on the weather nor the Sun and the Moon light. In principle they furnish the same detection ability for all the time and the directions of neutrino incidence.

For a high sensitivity detector which could detect single muons, a great number of downward muons become large background. On the contrary radio Cherenkov detector is immune from the muons. Of course it is a shortcoming to detect lower energy neutrinos in high statistics. If a UHE proton hits the atmosphere, it could not put the large energy deposit underground in a concentrated narrow region. Radiowave neutrino detector could sense only from many tracks of excess electrons inside the concentrated region with the help of strengthening by the coherence effect. Practically only UHE neutrino could induce electric field on the radio antennas underground.

In comparison with ice, rocksalt has 2.4 times higher density, shorter radiation length (1/3) and 1.4 times larger refractive index. Then high energy particle shower size is small owing to the high density. The Cherenkov angle

for electron is large and the threshold energy for electron is small due to the high refractive index. Consequently, Rock salt is adequite medium to get larger Cherenkov radiation power. As shown in fig. 4 the maximum electric field strength is estimated to be at 4.3 GHz without absorption in the rock salt taking into acount the short radiation length and the wavelength contraction due to the higher refractive index.

Normally, rocksalt is covered by thick soil which absorbs electromagnetic wave completely. Then SND is background free from natural or artificial radiowave coming from the surface of the earth. Therefore background is coming from blackbody radiation corresponding to the temperature of the surrounding rocks. As the remaining potential background, radiation may come from a seismic movement of surrounding rocks which may generate radiowave due to the piezoelectric effect by the stress in the rocks. If such a radiation could be detected, the observation contributes to the seimology.

2-3. Appearance of tau neutrino due to oscillation

Detection of high-energy cosmic tau neutrinos [16] could be achieved by making use of the characteristic double shower events [17] in the detector medium. They are connected by a μ like track. The size of the second bang is on the average a factor of two larger than the first bang. Electron neutrinos produce a single bang at these energies whereas the muon neutrinos typically produce a single shower along with a zipping μ -like track. Based on these rather distinct event topologies, cosmic neutrino flavor may be conceivable. We assume the standard ratio of the intrinsic cosmic neutrino flux is $F(\nu_e):F(\nu_\mu):F(\nu\tau)=1:2:0$. With the constraints of the solar and atmospheric neutrino and the reactor data, we obtain the ratio of the cosmic high-energy neutrino fluxes in the far distance is 1:1:1, irrespective of which solar solution is chosen.

[Fig. 6]

3. Possible experimental sites of rock salt mine and SND

We searched a medium which has long attenuation length in a Science chronological table [18]. Then we found rock salt is one of the lowest tanδ of 5-1 x 10^{-4} in the wide range in the radio frequency of 1kHz-10GHz with the relative real permittivity of 5.9. The loss angle tanδ is the ratio of imaginary divided by real part in the complex permittivity. The imaginary part presents the absorption in the material. Therefore smaller tanδ means longer

absorption length. The next idea comes from a finding that rock salt is free from water permeation described in a Topography dictionary [19]. On the salt dome, petroleum or natural gas are likely to deposite. They are covered with soil which prevents radiowave to penetrate from the surface.

[Fig. 7]

Due to this character, recently they are used to maintain radiation wastes, e.g. Asse and Gorleben salt mine in Germany, and WIPP (Waste Isolation Pilot Plant) at USA. Some laboratory measurements of RF complex permittivity have been made on a variety of rocks encountered in mining , tunneling, and engineering works. An RF impedance bridge and a parallel-plate capacitance test cell were employed at frequencies of 1,5, 25, and 100MHz [20]. In their measurement rock salt was the most transparent for the radiowave.

Rock salt had beem made in old days, around 250millions yeas ago when a huge ocean was situated in a hot , dry desert climate. As the water in a closed region evaporate, dissolved substances are left behind Salt consists of the two bacis elecments, sodium and chlorine, and forms colourless, cube-like crystals. Various additional elements such as iron, potassioum, magnesium or calcium, discolour the slat and also alter its taste; magnesium produces a bitter taste and potassium a soapy one.

There are many rock salt basins in the world [21].

[Fig. 8a, 8b]

Unfortunately there is no rock salt in Japan. In that era, Japan has no chance to form rock salt since it is under the ocean. We visited five rock salt mines, Hallein and Altaussee at Salzkammergut near Saltzburg, Austria July 1999. The Hallein already closed mining 10 years ago and active only for sight seeing. The Altaussee is still active to produce salt by borehole brine method. The diameter of rock salt is around 2km at Altaussee rock salt mine. The entrance of the salt mine is located at the mountain side going into horizontally. An Austrian expert said it is the largest and the cleanest among Europian Alps rock salt mines. But their tunnels inside were wetty and the temperature was 5-10°C. There were lakes underground. Tourist could ride on a boat on the lake. As far as the view from the sight-seeing course, it seems it was not adequate for the radiowave detection since the water penetrating the salt may absorb radiowave much.

We visited Asse research mine Mar. 2000 located near Braunschweig between Hanover and Berlin, Germany. This is an underground laboratory as a service facility of the GSF-National Reserch Centre for Environment and Health. Most of the tunnels would be used to store radiation wastes. We could go down driving a car as well as by a facility of elevator. The tunnel goes down to 1000 m with a lot of horizontal tunnels from the surface. Air was sent inside to cool down the temperature and the humidity was low. Near the bottom there was a low background radiation laboratory operated by PTB (the Physikalisch-Technische Bundesanstalt in Braunschweig, Germany).

In the rock salt environment, natural radiation background from uranium and thorium is lower than inside of normal rocks. In Asse mine, a group from Hannover studied the salt bodies for the repositories for nuclear wast using a 50 MHz ground-penetrating radar. They have succeeded to analyse the body in tomographically [22].

[Fig. 9a, 9b,9c]

The Hockley salt mine is near Houston, Texas. The salt mining is executed for commercial use. It seems enough sized salt dome for the neutrino detector. There is an underground "The Hockley Seismic Station" operated by the Institute for Geophysics, University of Texas and is a cooperative project between the University Of Texas, IRIS, USNSN, and the United Salt Corporation. The Hockley seismometer is located in an excavated chamber within an active salt mine owned by United Salt Corporation. The chamber lies approximately 470 meters below the surface within a large salt dome. Locating the instrument within a salt dome reduces the noise from human activity that generally affects instruments on the surface. The air was dry and the temperature was rather high.

The Waste Isolation Pilot Plant, or WIPP, is the first underground repository licensed to safely and permanently dispose of transuranic radioactive waste left from the research etc in USA. After more than 20 years of scientific study, public input, and regulatory struggles, WIPP began operations on March, 1999. It is located in the remote Chihuahuan Desert of Southeastern New Mexico, project facilities include disposal rooms mined 540m underground in a 500m thick salt formation that has been stable for more than 200 million years. Over the next 35years, WIPP is expected to receive shipments. The temperature of the rock salt is 24°C and the air was dry. The rock salt extends horizontally in the wide range although the salt deposite is not so deep. There is enough land of the govermental property to construct SND.

[Fig. 10a, 10b, 10c]

SND is envisaged as shown in fig. 11. Radio sensors of 216 are arrayed regularly in 200m repetition inside a 1km x 1km x 1km rock salt. The attenuation length of 400m at 1 GHz needs the sensor separation distance of 200m as well as to detect the Cherenkov ring shape. Six radio sensors are hung on a string. The string is lowered in a well with the depth of over 1km. At the total 36 wells should be bored.

[Fig. 11]

4. Measurement of microwave absorption length in the laboratory and the noise measurement of a radiometer

We have measured RF complex permittivity of a few rock salt samples from Hallstadt salt mine [(1)200mm x 200mm x 11mm, (2)200mm x 200mm x 30mm], Austria and Asse salt mine [(3)200mm x 200mm x 99mm], Germany. They are shown in Fig. 12a and 12b.

[Fig. 12a, 12b]

The method is so called free space measurent at 9.4GHz in a non-destructive manner [23]. The measurement was done by a vector network analyzer HP85107A. The microwave was radiated downward with the incident angle of 5° to a sample by a horn antenna having an aperture of 97mm x 68mm. The reflected radiowave was detected by another horn antenna of the same aperture with the angle of 5°. The distance from the horn antennas to the sample was 1.3m. A method using metal-plate reflector of 200mm x 200mm x 3mm with or without on the upper surface of a sample was developed in order to provide a non-destructive way for the assessment of microwave materials in free space. The distance from the antennas was adjusted to keep the same in the two cases of with and without the metal plate. The sample was placed horizontally on the metal plate of the same size. By displacing the position of the metal-plate reflector on the specimen to be tested, the incident wave and the scattered wave from the measured area were determined without the influence of extraneous waves such as the direct coupling between transmitting and receiving anntennas and scattered waves from background objects. Because the behaviour of a metal-plate reflector is similar to that of an optical shutter in optics.

[Fig. 13a, 13b]

The measurement was done at each position of the sample being separated in 2mm which corresponds to 50° change in phase. The measured complex values of recieved signal are plotted in the fig. 14 in each position with (solid line) and without (dotted line) metal plate.

[Fig. 14]

The upper figure is in parallel and downward in perpendicular polarization with the scattering plane. Naively, in case of single reflection at the bottom surface of the sample, the angle and the radius differences in the complex plane correspond to real and imaginary permittivity, respectively. In more precise analysis, we take into account the multiple paths between the upper and the lower surfaces inside the sample. The complex permitivity was deduced from the ratio of the complex measurement of electric field with and without the metal plate. The measured real part of the complex permittivities are shown in table 2 with the linear polarization of parallel Rp and perpendicular Rs with the scattering plane. The values are well consistent with the value of 5.9 tabulated in the handbook [18]. For the imaginary part of the permittivity, The measurement accuracy is not enough

and we could say only they are equal or under ~6×10^{-4}, namely tanδ is equal or under ~1×10^{-4}.

Table 2. Real part of complex permittivities in rock salts:

Thickness / Polarization	Rp	Rs
Hall Statt 11.1mm	5.9	6.0
Hall Statt 30.1mm	5.9	6.0
Asse Mine 99.0mm	5.9	5.9

We could calculate the absorption coefficient α as:

$\alpha = (\omega/c)(\varepsilon'^{1/2})(\tan\delta)/2$
$= (2\pi)(10^{10})/(3\times10^{8})\ (6^{1/2})(1\times10^{-4})/2$
$= 2.5\times10^{-2}$,
where the notations are following:
complex permittivity; $\varepsilon = \varepsilon' - j\varepsilon'' = \varepsilon'(1-j\tan\delta)$,
loss angle in the permittivity; $\tan\delta=\varepsilon''/\varepsilon' =1\times10^{-4}$,
complex refractive index; $n = \varepsilon^{1/2} = (\varepsilon' - j\varepsilon'')^{1/2} =\varepsilon'^{1/2}(1-j\tan\delta)^{1/2}$.
Then absoption length becomes,
$1/\alpha$ = 40m at 10GHz
If we believe tanδ is constant with respect to the frequency, we get:
$1/a$ = 400m at 1GHz.

The preliminary results of the radiowave absorption length in the rock salt show that it has a chance to be used as the medium of UHE neutrino detector. We need to measure in the lower frequency and more samples to deduce the concrete conclusion. Further we are planning to measure natural rock salt samples by a perturbed cavity resonantor method at 9.4GHz [24].

[Fig. 15a, 15b]

By that method we already have got the result with a synthetic rock salt sample of 1mm x 1mm x 10mm as $5.8 - j3.5\times10^{-4}$, $\tan\delta = 0.6\times10^{-4}$ which is consistent with the values of the free space measurent at 9.4GHz in a non-destructive manner and the ref. [18]. Although, in the natural rock salt sample it is rather difficult to cleave to the size.

We have tested a noise level of a radiometer system. The main part the radiometer is a modified TV Broadcasting Satelite (BS) reciever [25], namely an amplifier-converter module with the center frequency of 10.6GHz. The system is composed of the horn antenna having the aperture of 97mm x 68mm, the amplifier-converter module, an 30dB amplifier, a rectifier and a time chart recorder or an oscilloscope. The amplifier-converter module consists of a signal conversion part from the waveguide of the horn antenna to a coaxial style, 3 stage low noise HEMT amplifier with filter at the center

frequency of 10.6 GHz (band-width of 200 MHz), and frequency converter to whom the local oscillator signal of 9.6 GHz is introduced from outside. After the conversion part, the signal is amplified with a 3 stage amplifier in the module. The horn antenna is directed vertical to the sky having around a 30K noise or covered with 300K thermal noise source. The comparison of the signals, we could get the the noise level of the amplifier-converter module as low as 150K. We get the noise level well below the rock salt temperature with the modified BS reciever used by popular TV audience. Due to the results we could afford to get a lot of the recievers with low cost.

Summary

Rock salt is studied as a radiowave transmission medium in a UHE cosmic neutrino detector. The radiowave would be generated by Askar'yan effect (negative excess charges in the electromagnetic shower with coherent Chrenkov radiation) in the UHE neutrino interaction in the rock salt. Some rock salt mines are investigated whether it has a possibility as a SND site or not. We found there are potential sites to construct SND. The samples of the rock salts are gathered to measure the absorption length. As a tentative result, the absorption length of the radiowave is obtained around 400m at 1Ghz. The configuration of antennas with 200m spacing in a 1km x 1km x 1km rock salt are studied taking into the attenuation and the radiation pattern of the coherant Cherenkov radiation. A radiometer modified from TV BS reciever showed the noise level of 150K which is enough low for the measurement. It is an advantage that a relatively low cost reciever could be used in a large number of arrays.

Before the site is decided, it is important to measure the absorption length in situ. There may be defects and impurities as well as intrusions by rocks other than salt. For that research it is useful to employ the ground penetrating radar which is well explored technique. Further it is indispensable to measure the coherent Cherenkov radiation due to a pulsed electron beam supplied by an acceralator. By the measurement we could calibrate to know the energy of the initial electromagnetic shower which depends on how much coherency is realized.

Acknowledgements

This work was supported partly by Funds for Special Research Project at Tokyo Metropolitan University, Fiscal Year 1999. We should appreciate Prof. K.Minakata (TMU) to support this project.

We express our gratitude to M.E. Ryouichi Ueno who discussed with and advised us about the microwave techniques. He was indispensable to carry out this study.

This study could not be possible without the assistances from and discussions with many other peoples. Since a part of the field researched was far from our major. Here we express our appreciations to those who have interests and extended his favor on our research.

References

[1]F.W.Stecker, C.Done, M.H.Salamon and P.Sommers, Phys. Rev. Lett. 66 (1991) 2697-2700.

[2]S.Barwick, F.Halzen, D.Lowder, T.Miller, R.Morse, P.B.Price and A.Westphal, J.Phys. G:Nucl. Part. Phys. 18(1992)225-247; Thomas K.Gaisser, Francis Halzen, Todor Stanev, Phys. Reports 258(1995)173-236.

[3]M.Takeda et al, Phys. Rev. Lett., 81(1998)1163.
[4] K.Greisen, Phys. Rev. Lett. 16(1966)748; G.T.Zatsepin, V.A.Kuzumin, Sov. Phys. JETP Lett. 4(1966)78.

[5]G.Burdman, F.Halzen and R.Gandhi, Phys. Lett.B417(1997)107-113; P.Jain, Douglas W.Mckay, S.Panda, John P.Ralston, Phys. Lett. B484 (2000) 267-274.

[6]Raj Gandhi, Chris Quigg, Mary Hall Reno and Ina Sarcevic, Astroparticle Phys. 5(1996)81-110; Phys. Rev.D58, 093009: Gunter Sigl, Phys. Rev. D57 (1998) 3786-3789: J.Kwiecinski, A.D.Martin, A.M.Stasto, Phys. Rev.D59, 093002 (1999); R.Horvat, Phys. Lett. B480(2000)135-139.

[7]Athar Husain, Presentation at the seminar of high energy theory group, Oct. 2000, TMU.
[8] SuperK Collaboration, Y.Fukuda et al., Phys. Rev. Lett. 81, 1562 (1998).

[9]G.A.Askar'yan, Soviet Physics JETP 41(1962)616; 48(1965)988.
[10]L.Landau, I.Pomeranchuk, Kokl. Akad. Nauk SSSR92(1953)535; 92(1935)735; A.B.Migdal, Phys. Rev.103(1956)1811; Ah.Eksp. Fiz. 32(1957)633 [Sov. Phys. JETP 5 (1957)527]; Spencer Klein, Rev. Mod. Phys. 71(1999)1501.

[11] Ter-Mikaelian (1953)
[12]M.A.Markov and I.M.Zheleznykh, Nucl. Instrum. Methods. A248 (1986) 242-251.

[13]F.Halzen, E.Zas, T.Stanev, Phys. Lett. B257(1991)432; E.Zas, F.Halzen, T.Stanev, Phys. Rev. D45(1992)362; J.Alvarez-Muniz and E.Zas, Phys. Lett.B411(1997)218-224; George M.Frichter, John P.Ralston and Douglas W.Mckay, Phys. Rev.D53(1996)1684.

[14]The most recent status of large high-energy neutrino detectors are shown in the presentation transparencies in 19th International Conference on Neutrino Physics and Astrophysics (Neutrino 2000), 2000, Sudbury, Canada at URL http://ALUMNI.LAURENTIAN.CA/www/physics/nu2000/.

[15]Peter Gorham, David Saltzberg, Paul Schoessow, Wei Gai, John G.Power, Richard Konecny and M.E.Conde, hep-ex/0004007.

[16]F.Halzen, D.Saltzberg, Phys. Rev.Lett., 81(1998)4305.
[17]J.G. Lerarned and S.Pakvasa, Astropart. Phys. 3, 267(1995); H.Athar, M.Jezabek and O.Yasuda, Phys. Rev. D62,103007 (2000); Athar Husain, hep-

ph/9912417, 1999; Athar Husain, Nucl. Phys. B(Proc. Suppl.)76(1999)419; H. Athar, G.Parente and E.Zas, hep-ph/0006123, 2000.

[18]Science chronological table edited by the Japanese National Astronomical Obsevatory (in Japanese).

[19] Topography dictionary publised by Ninomiya Book Co. (in Japanese)
[20]John C.Cook, Geophysics, Vol. 40, No.5, 1975, 865-885.
[21]Handbook of World Salt Resources, Stanley J. Lefond, Plenum Press, New York, 1969; Salt Domes, Michel T. Halbouty, Gulf Publishing Company, 1979.

[22] E.Mundry, R.Thierbach, F.Sender and H.Weichart, Proceedings of the SixthInternational Symjposium on Salt, 1983 Vol.I, 585-599; H.Nickel, F.Sender, R.Thierbach and H.Weichart, Geophysical Prospecting 31, 131-148, 1983; Motoyuki Sato and Rudolf Thierbach, IEEE Transactions on Geioscience and Remote Sensing, Vol.29, No.6, 1991, 899-904; D.Eisenburger, , Proceedings of the 5th International Conference on Ground Penetrating Radar, 1994, 647-659;D.Eisenburger, V.Gundelach, F.Sender, R.Thierbach, Proceedings of the 6th International Conference on Ground Penetrating Radar, 1996, 427-432.

[23]Ryouichi Ueno and Toshio Kamijo, IEIC Trans. Commun. E83B(2000)1554-1562; Ryouichi Ueno and Toshio Kamijo, Memoirs of Graduate School of Engineering, Tokyo Metropolitan University, No.48, 1998, pp5743-5752 (1999-02).
[24]Ryouichi Ueno and Toshio Kamijo, Memoirs of Faculty of Tech., Tokyo Metropolitan University, No.38, 1988, pp.3923-3933, March 1989.
[25]The amplifier-converter was transferred from Prof. T.Daishido of Wasada University, Tokyo.

Figure captions

Fig. 1. Ultra high energy (UHE) cosmic neutrinos are expected from an active galactic nucleus nearly 100Mpc (10 million light years) far from the earth.
[7]Athar Husain, Presentation at the seminar of high energy theory group, Oct. 2000, TMU.

Fig. 2. Neutrino-nucleon interaction cross sections at high energies. Differential shadow factor by the earth is also presented.
[6]Raj Gandhi, Chris Quigg, Mary Hall Reno and Ina Sarcevic, Astroparticle Phys. 5(1996)81-110; Phys. Rev.D58, 093009.

Fig. 3. UHE neutrino flux estimates
[7]Athar Husain, Presentation at the seminar of high energy theory group, Oct. 2000, TMU.

Fig. 4. Total absolute tracklength and tracklength associated to charge exess in ice, electric field with respect to obsevation angle and frequency.
[13]F.Halzen, E.Zas, T.Stanev, Phys. Lett. B257(1991)432.

Fig. 5. Detected radiation energy against to the number of the electrons in a pluse. Coherence effect from an electron pulse is clearlyj shown.
[15]Peter Gorham, David Saltzberg, Paul Schoessow, Wei Gai, John G.Power, Richard Konecny and M.E.Conde, hep-ex/0004007.

Fig. 6. Appearance of tau neutrino due to oscillation. We assume the standard ratio of the intrinsic cosmic neutrino flux is $F(\nu_e):F(\nu_\mu):F(\nu\tau)=1:2:0$. With the constraints of the solar and atmospheric neutrino and the reactor data, we obtain the ratio of the cosmic high-energy neutrino fluxes in the far distance is 1:1:1, irrespective of which solar solution is chosen.

[7] Athar Husain, Presentation at the seminar of high energy theory group, Oct. 2000, TMU.

Fig. 7. Rock salt is free from water. On the salt dome, petroleum or natural gas are likely to deposite. They are covered with soil which prevents radiowave to penetrate from the surface.

[19]Topography dictionary publised by Ninomiya Book Co. (in Japanese).

Fig. 8a. Major salt basins in the eastern hemisphere.
[21]Handbook of World Salt Resources, Stanley J. Lefond, Plenum Press, New York, 1969; Salt Domes, Michel T. Halbouty, Gulf Publishing Company, 1979.

Fig. 8b. Major salt basins in the western hemispheres.
[21]Handbook of World Salt Resources, Stanley J. Lefond, Plenum Press, New York, 1969; Salt Domes, Michel T. Halbouty, Gulf Publishing Company, 1979.

Fig. 9a. Method of ground penetrating radar in salt domes.
[22] H.Nickel, F.Sender, R.Thierbach and H.Weichart, Geophysical Prospecting 31, 131-148, 1983.

Fig. 9b. Three-dimensional representation of ground-probing radar measurements.

[22] D.Eisenburger, , Proceedings of the 5th International Conference on Ground Penetrating Radar, 1994, 647-659.

Fig. 9c. View from the above and the side

Fig. 10a.The Waste Isolation Pilot Plant, or WIPP, is the permanently dispose of transuranic radioactive waste left from the research etc in USA. It is located in the remote Chihuahuan Desert of Southeastern New Mexico,
Fig. 10b. Structure of WIPP stratums.
Fig.10c. Spacial view of WIPP surface & underground facilities.
Fig. 11. Salt Neutrino Detector (SND) underground. Radio sensors of 216 are arrayed regularly in 200m repetition inside a 1km x 1km x 1km rock salt. Six radio sensors are hung on a string. The string is lowered in a well with the depth of over 1km. At the total 36 wells should be bored. A coherent Cherenkov radiation with the emission angle of 66 deg is generated by excess electrons in the shower in the UHE neutrino interaction.

Fig. 12a. Rock salt samples from Hallstadt salt mine [(1)200mm x 200mm x 11mm, (2)200mm x 200mm x 30mm], Austria.

Fig. 12b. Rock salt samples from Asse salt mine [(3)200mm x 200mm x 99mm], Germany.

Fig. 13a. Measurement of permittivity with a free space method at 9.4GHz in a non-destructive manner. The measurement was done by a vector network analyzer HP85107A. The microwave was radiated downward with the incident angle of 5° to a sample by a horn antenna having an aperture of 97mm x 68mm. The reflected radiowave was detected by another horn antenna of the same aperture with the angle of 5°. The distance from the horn antennas to the sample was 1.3m.
Fig. 13b. A photo of the measuring apparatus with a sample from Asse salt mine. [23]Ryouichi Ueno and Toshio Kamijo, IEICE Trans. Commun. E83B(2000)1554-1562; Ryouichi Ueno and Toshio Kamijo, Memoirs of Graduate School of Engineering, Tokyo Metropolitan University, No.48, 1998, pp5743-5752 (1999-02).

Fig. 14. The measurement was done at each position of the sample being separated in 2mm which corresponds to 50° change in phase. The measured complex values of recieved signal are plotted in each position with (solid line) and without (dotted line) metal plate. The upper figure is in parallel and downward in perpendicular polarization with the scattering plane. Naively, in case of single reflection at the bottom surface of the sample, the angle and the radius differences in the complex plane correspond to real and imaginary permittivity, respectively. In more precise analysis, we take into account the multiple paths between the upper and the lower surfaces inside the sample.

Fig. 15a . Permittivity measuring apparatus of a perturbed cavity resonator.

Fig. 15b. A photo of a perturbed cavity resonator.

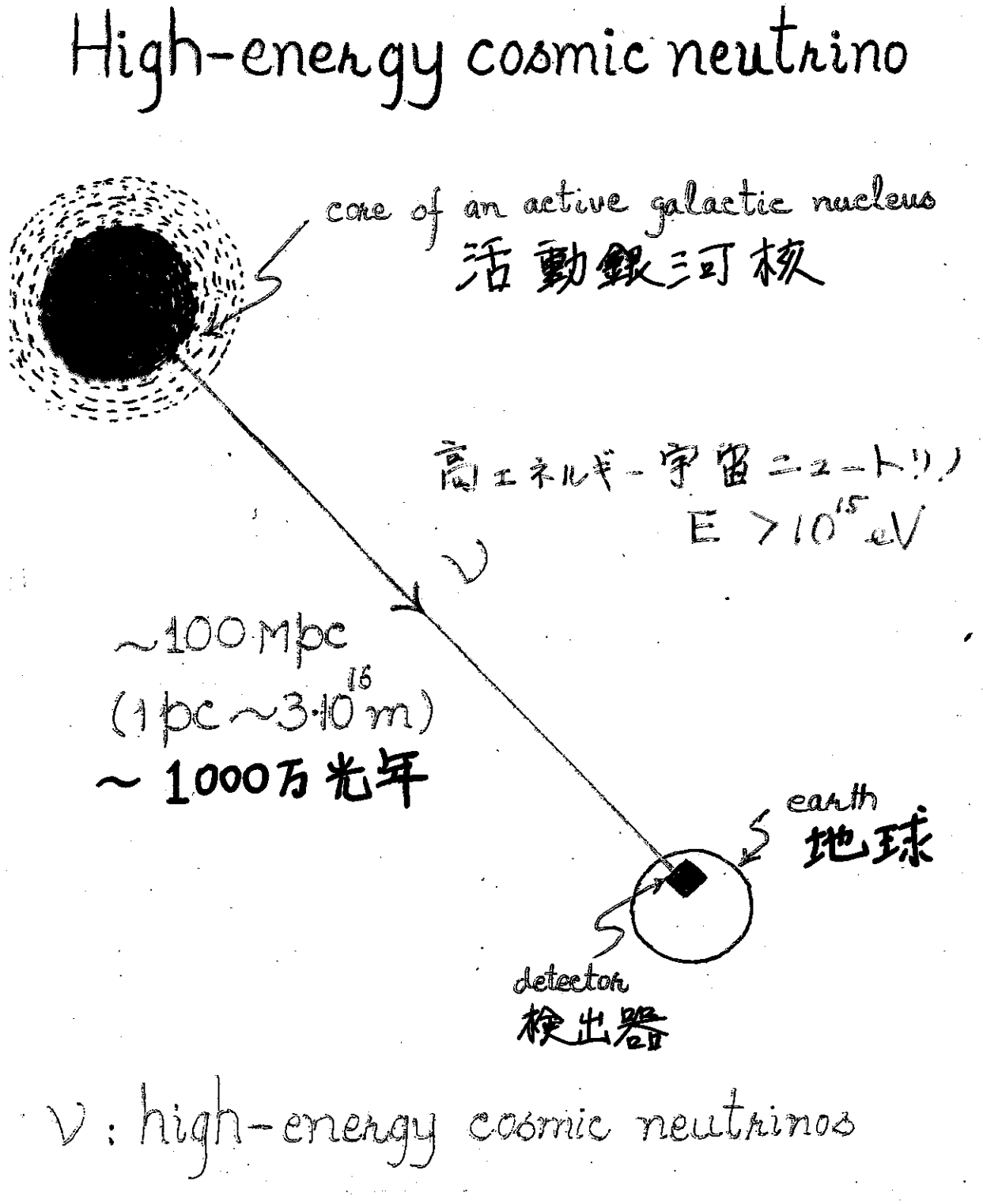

Fig. 1. Ultra high energy (UHE) cosmic neutrinos are expected from an active galactic nucleus nearly 100Mpc (10 million light years) far from the earth. [7]Athar Husain, Presentation at the seminar of high energy theory group, Oct. 2000, TMU.

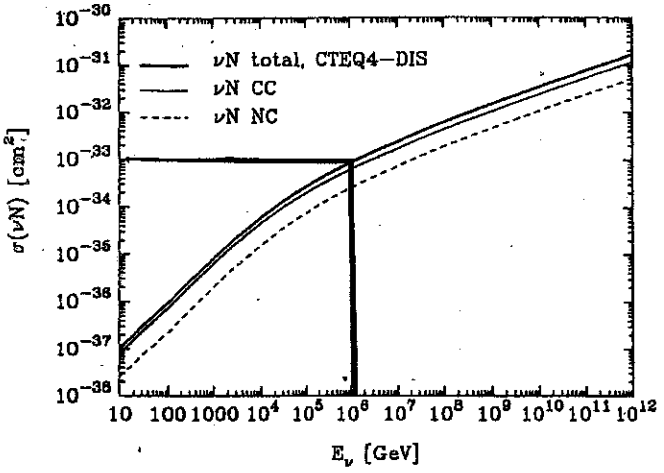

FIG. 1. Cross sections for $\nu_l N$ interactions at high energies, according to the CTEQ4-DIS parton distributions: dashed line, $\sigma(\nu_l N \to \nu_l + \text{anything})$; thin line, $\sigma(\nu_l N \to l^- + \text{anything})$; thick line, total (charged-current plus neutral-current) cross section.

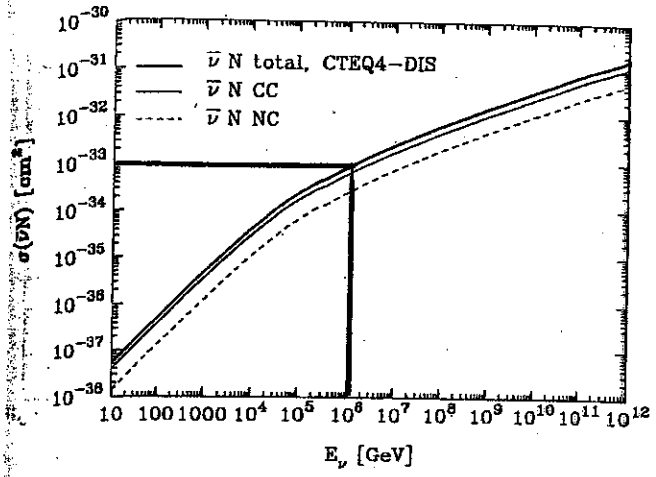

FIG. 3. Cross sections for $\bar{\nu}_l N$ interactions at high energies, according to the CTEQ4-DIS parton distributions: dashed line, $\sigma(\bar{\nu}_l N \to \bar{\nu}_l + \text{anything})$; thin line, $\sigma(\bar{\nu}_l N \to l^+ + \text{anything})$; thick line, total (charged-current plus neutral-current) cross section.

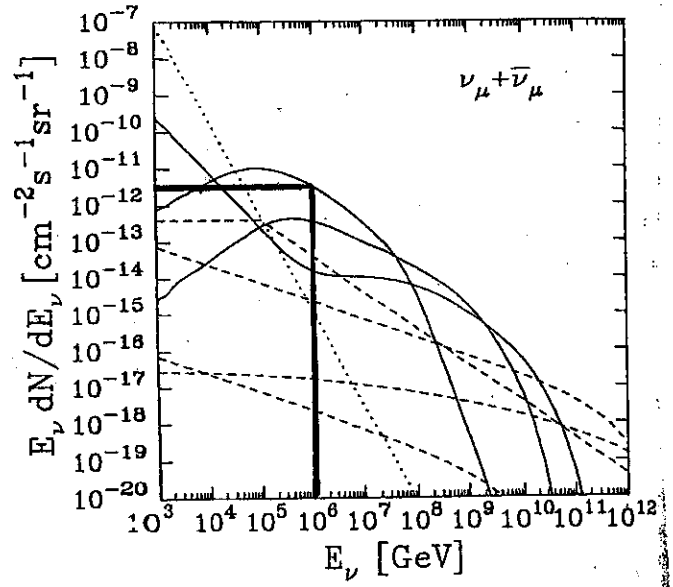

FIG. 9. Muon neutrino plus antineutrino fluxes scaled by neutrino energy at the Earth's surface. Solid lines represent AGN fluxes. In decreasing magnitude at $E_\nu = 10^3$ GeV, they are AGN-M95, AGN-SS91 scaled by 0.3, and AGN-P96 ($p\gamma$). The dashed lines, in the same order, represent the GRB-WB, TD-WMB12, TD-WMB16, and TD-SLSC fluxes. The dotted line is the angle-averaged atmospheric (ATM) neutrino flux.

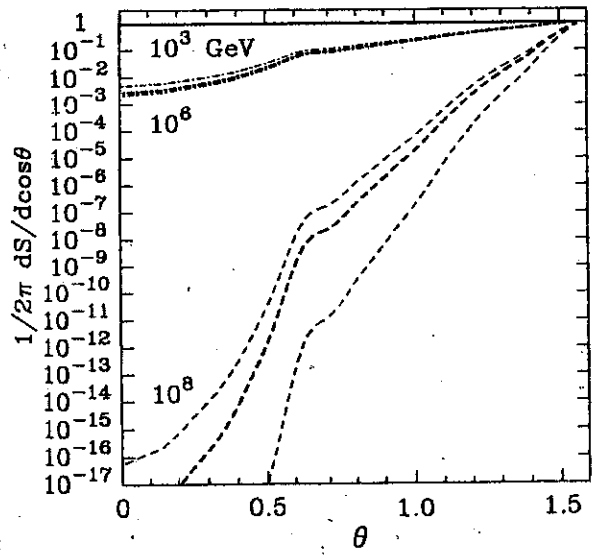

FIG. 10. Differential shadow factor $(1/2\pi)\, dS(E_\nu)/d\cos\theta$ *versus* nadir angle θ, for $E_\nu = 10^3$ GeV (solid line), 10^6 GeV (dot-dashed lines), and 10^8 GeV (dashed lines). For each neutrino energy, the thick line corresponds to the CTEQ4-DIS parton distributions; the upper and lower satellite lines correspond to the CTEQ3-DLA and MRS-D'_ parton distributions, respectively.

Fig. 2. Neutrino-nucleon interaction cross sections at high energies. Differential shadow factor by the earth is also presented.

[6] Raj Gandhi, Chris Quigg, Mary Hall Reno and Ina Sarcevic, Astroparticle Phys. 5(1996)81-110; Phys. Rev.D58, 093009.

Some flux estimates

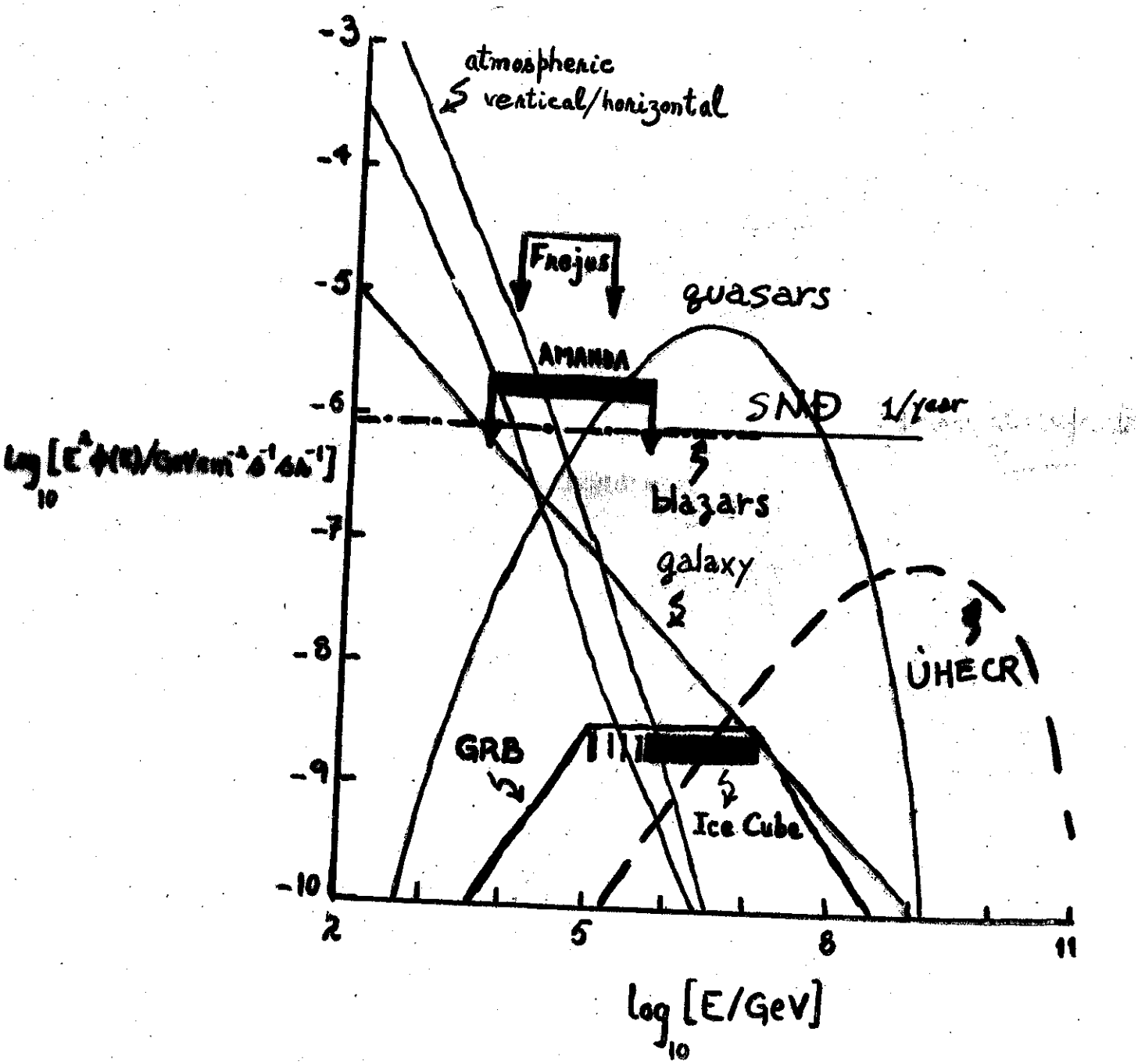

Fig. 3. UHE neutrino flux estimates

[7]Athar Husain, Presentation at the seminar of high energy theory group, Oct. 2000, TMU.

Volume 257, number 3,4 PHYSICS LETTERS B 28 March 1991

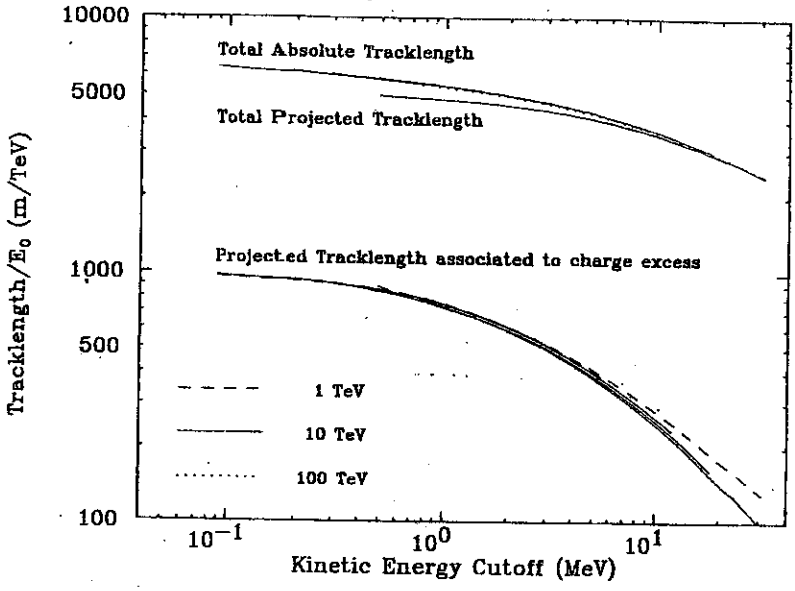

Fig. 1. Sum of tracklengths for all charged particles in 1, 10, and 100 TeV electron showers as a function of the calculational cutoff. The three sets of curves correspond to (i) the sum of the absolute tracklengths; (ii) the sum of the tracklengths projected onto the shower axis, and (iii) the difference of electron and positron tracklengths. Several showers are shown for 1 and 10 TeV primaries indicating the effect of fluctuations.

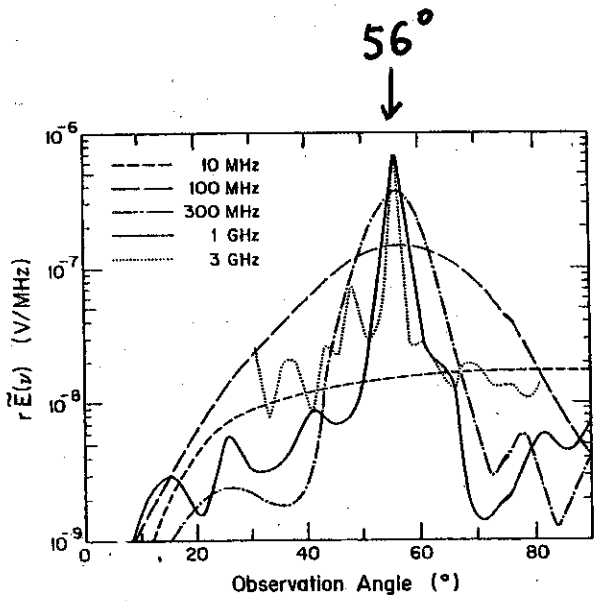

Fig. 2. Angular distribution of the electric field generated by a 10 TeV electron. The observation angle is the polar angle of the radiation with respect to the shower axis. The quantity $r\tilde{E}(\nu)$, distance times electric field, is related to power by eq. (6).

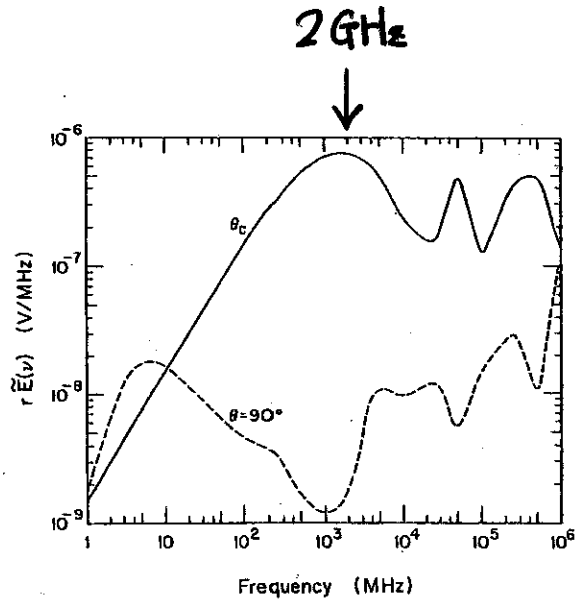

Fig. 3. Frequency spectrum of the electromagnetic pulse generated by a 10 TeV electron for two observation angles relative to the shower axis; θ_C is the Čerenkov angle.

Fig. 4. Total absolute tracklength and tracklength associated to charge exess in ice, electric field with respect to obsevation angle and frequency.

[13]F.Halzen, E.Zas, T.Stanev, Phys. Lett. B257(1991)432.

Radio-Frequency Measurements of Coherent Transition and Cherenkov Radiation: Implications for High-Energy Neutrino Detection

Peter Gorham[3], David Saltzberg[2], Paul Schoessow[1], Wei Gai[1], John G. Power[1], Richard Konecny[1], and M. E. Conde[1]

B. Coherence of TR

A crucial feature of this radio emission necessary for its application to detection of high energy particles is its coherence. Figure 5 shows the behavior of the detected power as a function of beam current for the no-target configuration where the radiation is expected to be primarily TR. Here the top points are from the dipole measurements, again at an angle of 70° from the beampipe end. The lower points are for the horn measurements, here all taken at an angle of 45° from the beampipe end. The solid lines have a slope of 2, representing the expected behavior for power proportional to N_e^2 (full coherence).

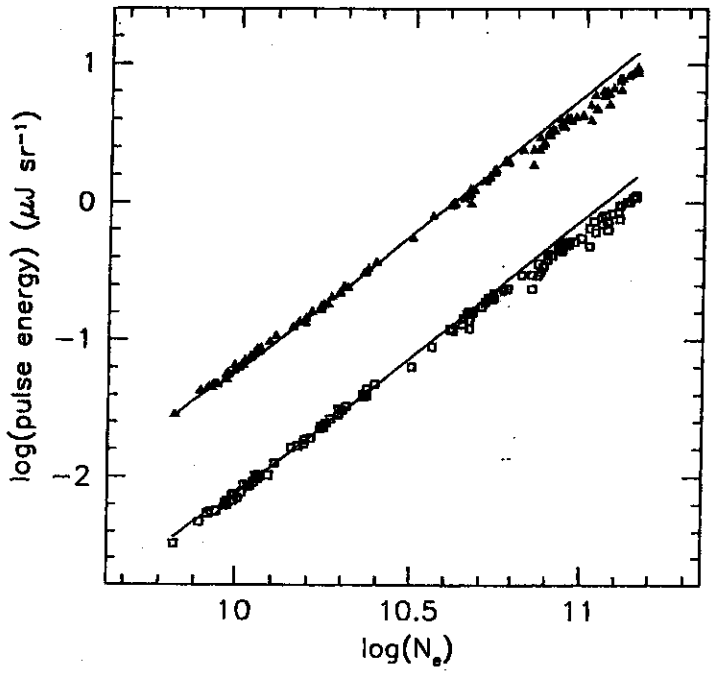

FIG. 5. Detected energy per pulse as a function of beam current. The upper points correspond to the dipole and the lower points the horn. In this configuration, the primary radiation is expected to be transition radiation from the Al vacuum window. The solid lines are the N_e^2 behavior if full coherence obtains, normalized to the lowest beam currents.

Fig. 5. Detected radiation energy against to the number of the electrons in a pluse. Coherence effect from an electron pulse is clearlyj shown.

[15]Peter Gorham, David Saltzberg, Paul Schoessow, Wei Gai, John G.Power, Richard Konecny and M.E.Conde, hep-ex/0004007.

$$2 \cdot 10^{6} \leq \frac{E_{\nu}}{GeV} \leq 2 \cdot 10^{7}$$

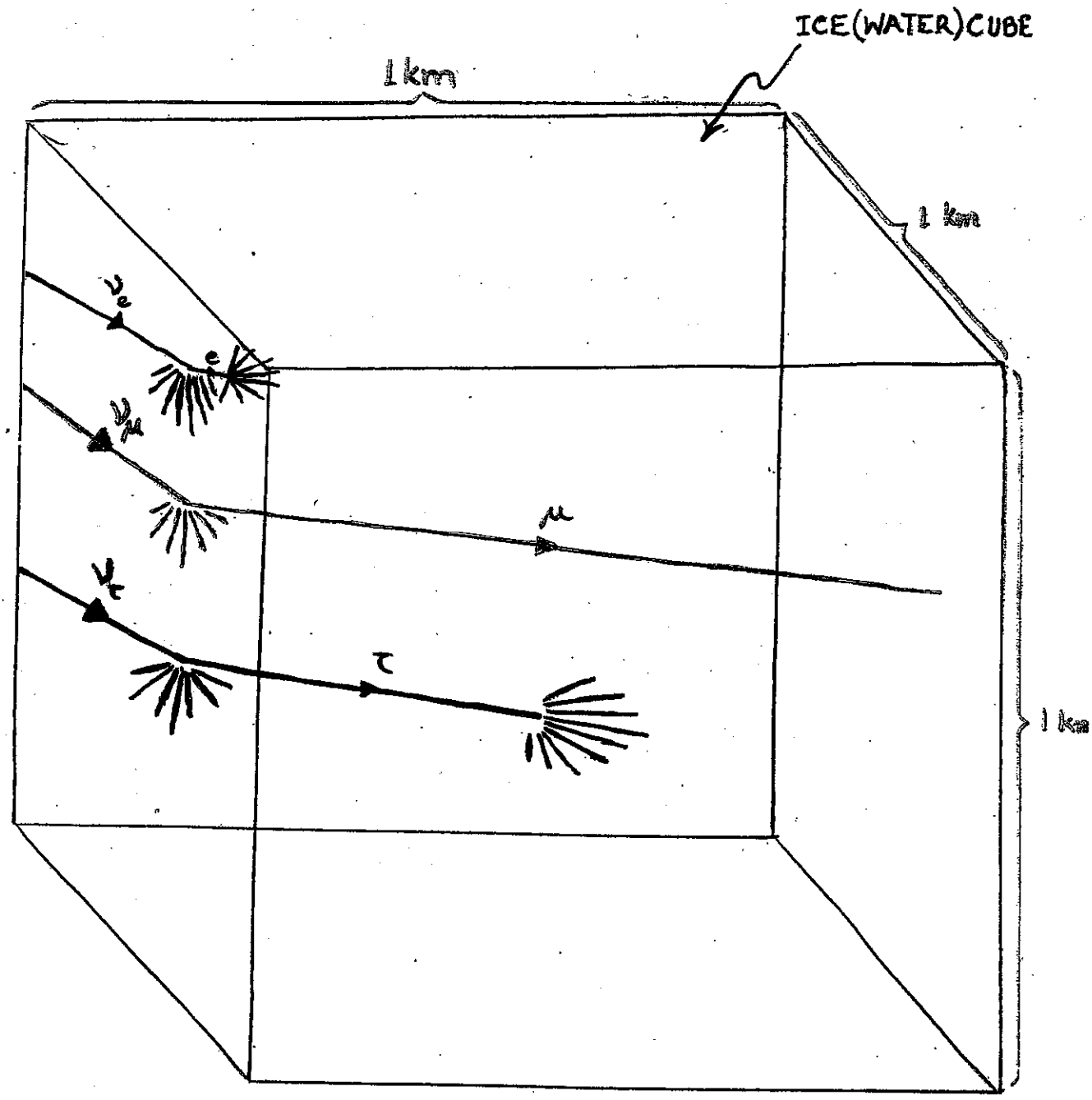

Fig. 6. Appearance of tau neutrino due to oscillation. We assume the standard ratio of the intrinsic cosmic neutrino flux is $F(\nu_e):F(\nu_\mu):F(\nu\tau)=1:2:0$. With the constraints of the solar and atmospheric neutrino and the reactor data, we obtain the ratio of the cosmic high-energy neutrino fluxes in the far distance is 1:1:1, irrespective of which solar solution is chosen.

[7] Athar Husain, Presentation at the seminar of high energy theory group, Oct. 2000, TMU.

岩　塩　(E) halite, rock salt　(G) Ste'nsalz　(F) sel gemme

NaCl，等軸晶系，普通は立方体結晶，硬度 2，比重 2.168，ガラス光沢を有し，無色・白・赤・青・黄などの色を示す．海水の蒸発では最後に沈殿する．ゴンドワナ大陸時代のペルム～三畳紀に大量の岩塩が堆積したが，北海周辺の Zechstein 岩塩はとくに有名．岩塩層が厚い砕屑岩におおわれると塑性流動してダイアピールをつくり，その周りには石油・天然ガスの貯留構造が発達しやすい．また透水率ゼロという特性を利用して産業廃棄物の封じ込みや液体燃料の一時的貯留のために利用されるようになった．ギリシア語の hals (海)から命名．

【文 献】Borchert, H., Muir, R. O. (1964): Salt deposits. (London, D. van Nostrand)　(岡田博有)

岩塩栓 (E) salt plug (G) Salzstock, Salzhorst (F) dôme de sel　地下深所に堆積していた岩塩が，上に堆積した泥岩や砂岩の荷重圧で堆積岩中の弱線に沿って上昇して生じた，煙突状の岩塩岩体のこと．岩塩栓上部周辺の堆積岩層はドーム状ないし背斜状に褶曲(ダイアピル褶曲diapir fold，注入褶曲 injection fold，穿孔褶曲 piercement fold，piercing fold)する．その堆積岩の示すドーム状構造，あるいは地表に現れたドーム状地形を岩塩ドーム (salt dome)という．

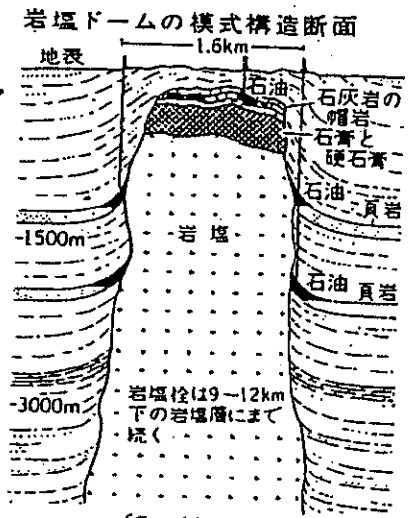

地表からの電波シールド
Radiowave shield from the surface

ときに岩塩栓を岩塩ドームとよぶこともある．岩塩栓は通常，頂部に石膏や硬石膏からなる板状の岩層をもち，その上に石灰岩からなる帽岩(cap rock)を載せている．この石灰岩中の空隙には石油が集まっていて，油田となることが多い．メキシコ湾岸油田やペルシア湾岸油田は，岩塩ドームの分布地域に発達している．

【文献】Harrison, J. V. (1930): The geology of some salt-plugs in Laristan. (Southern Persia). Quart. Jour. Geol. Soc. London, 86.　(寿円晋吾)

Fig. 7. Rock salt is free from water. On the salt dome, petroleum or natural gas are likely to deposite. They are covered with soil which prevents radiowave to penetrate from the surface.

[19]Topography dictionary publised by Ninomiya Book Co. (in Japanese).

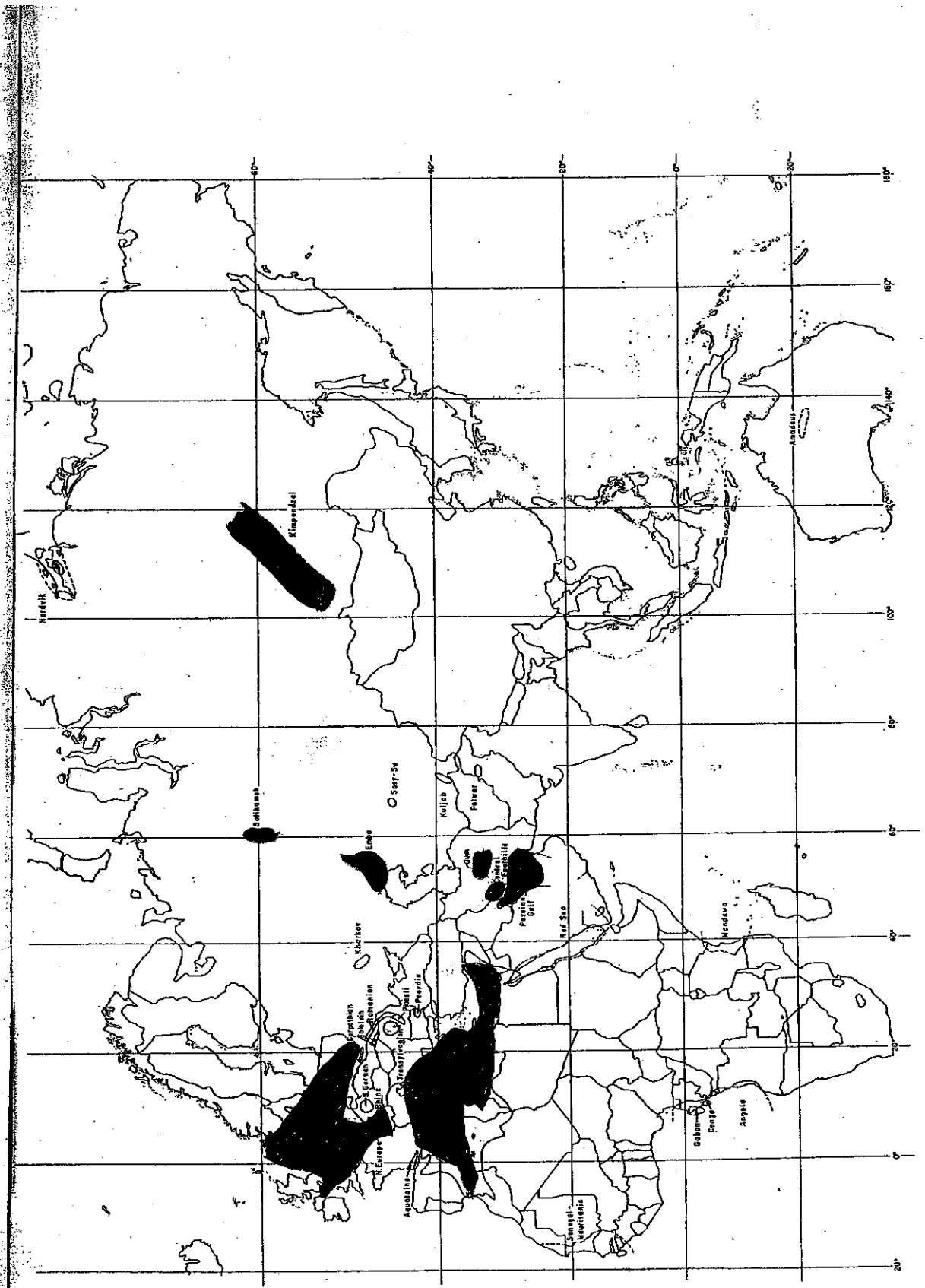

Figure 1-1. Map shows location of major salt basins in the Eastern Hemisphere. The depositional habitat of salt deposits include: salt basins containing bedded salt which is essentially little deformed or, if folded, is the result of basin tectonics (compression, tension, shear); salt dome basins containing salt controlled structures where isostatic salt movement has created the structural form. (Modified in part after Eby, 1956)

Fig. 8a. Major salt basins in the eastern hemisphere.
[21]Handbook of World Salt Resources, Stanley J. Lefond, Plenum Press, New York, 1969; Salt Domes, Michel T. Halbouty, Gulf Publishing Company, 1979.

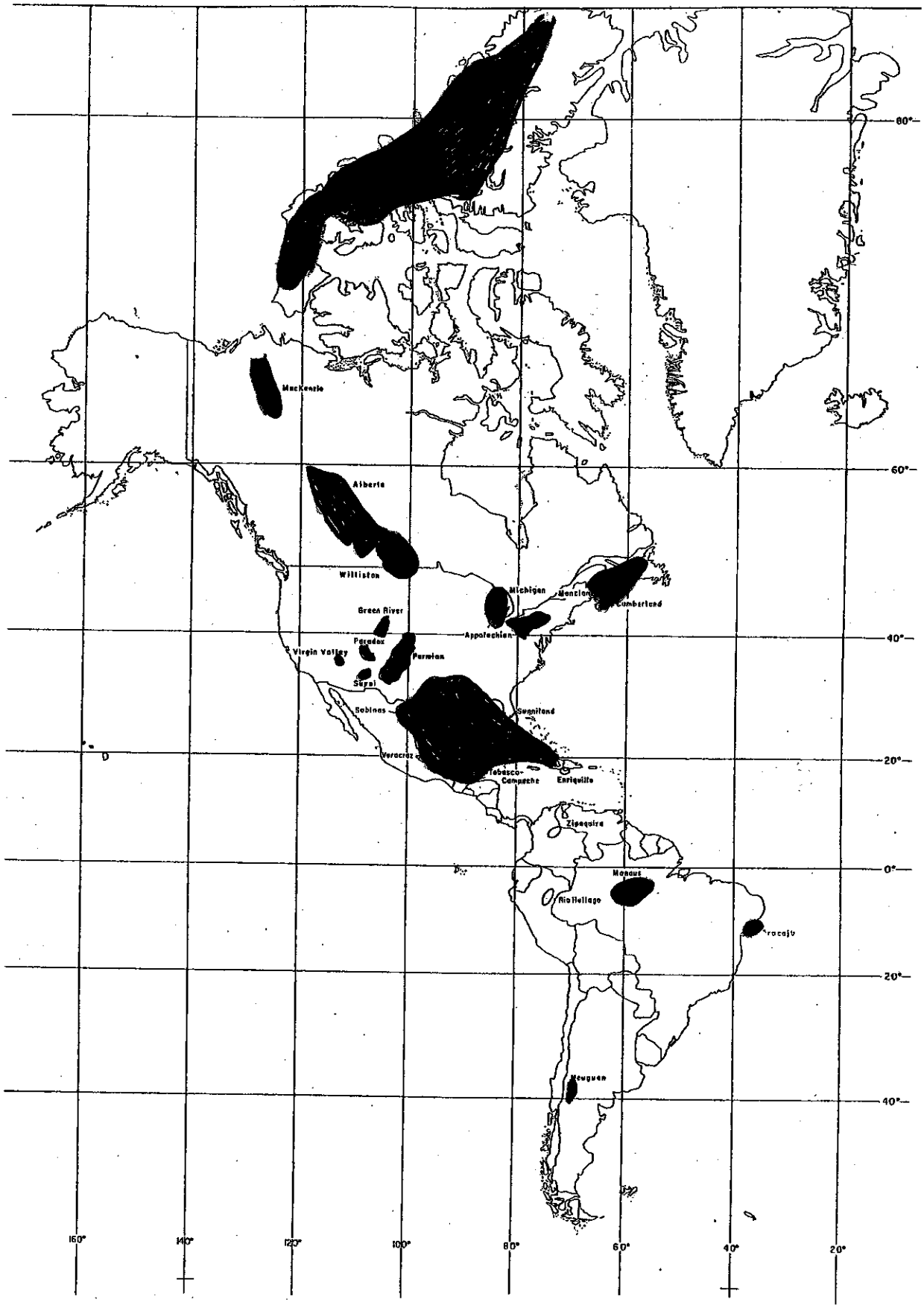

Figure 1-2. Map shows location of major salt basins in the Western Hemisphere. The Gulf Coastal province of the United States contains five separate salt dome basins within the larger Gulf region salt basin.

Fig. 8b. Major salt basins in the western hemispheres.
[21]Handbook of World Salt Resources, Stanley J. Lefond, Plenum Press, New York, 1969; Salt Domes, Michel T. Halbouty, Gulf Publishing Company, 1979.

EXPLORING THE INTERIOR OF SALT DOMES FROM BOREHOLES*

H. NICKEL,** F. SENDER,*** R. THIERBACH**** and H. WEICHART***

INTERIOR OF SALT DOMES

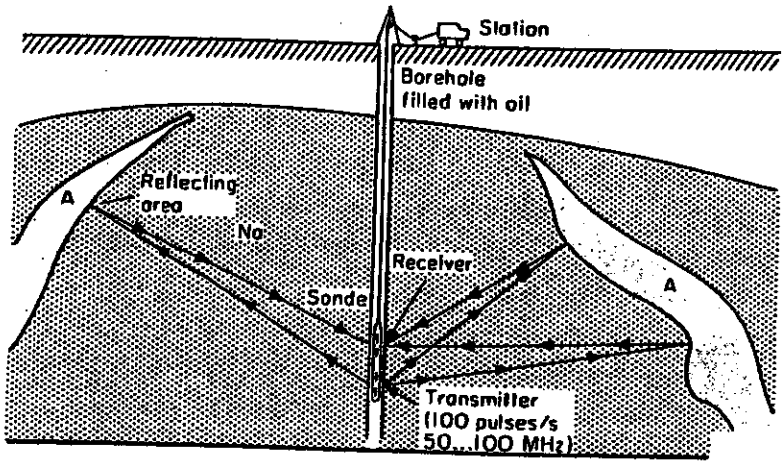

Fig. 2. Electromagnetic HF reflection method in salt.

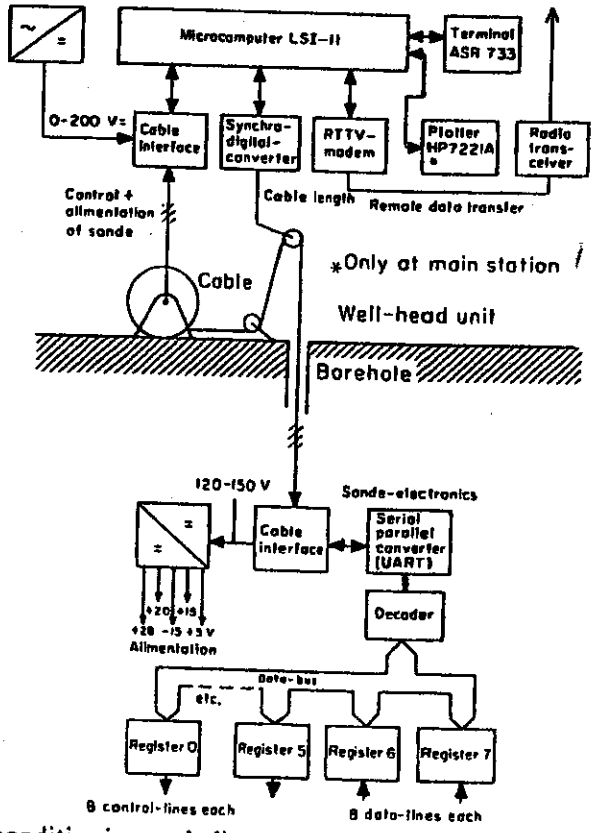

Fig. 3. Signal conditioning and alimentation for HF well-logging equipment.

Fig. 9a. Method of ground penetrating radar in salt domes.

[22] H.Nickel, F.Sender, R.Thierbach and H.Weichart, Geophysical Prospecting 31, 131-148, 1983.

RADAR MEASUREMENTS

Dieter Eisenburger[1]

1, 2, 4, 5, 6 : Drifts
3, 7, 8, 9 : Anhydrite layer

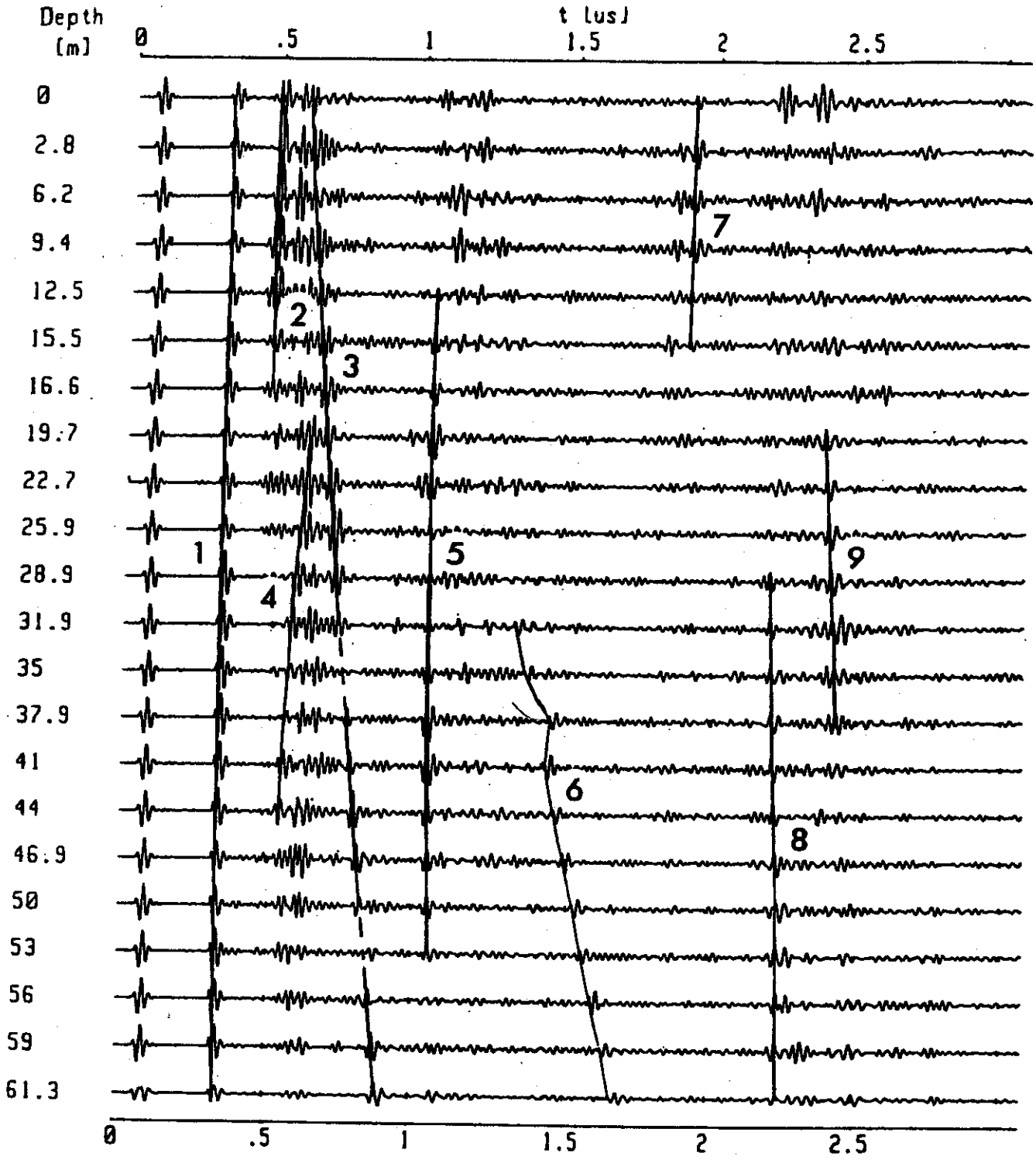

Fig. 9b. Three-dimensional representation of ground-probing radar measurements.

Fig. 5: Borehole radar profile (dipole signal) with the picked reflectors.

[22] D.Eisenburger, , Proceedings of the 5th International Conference on Ground Penetrating Radar, 1994, 647-659.

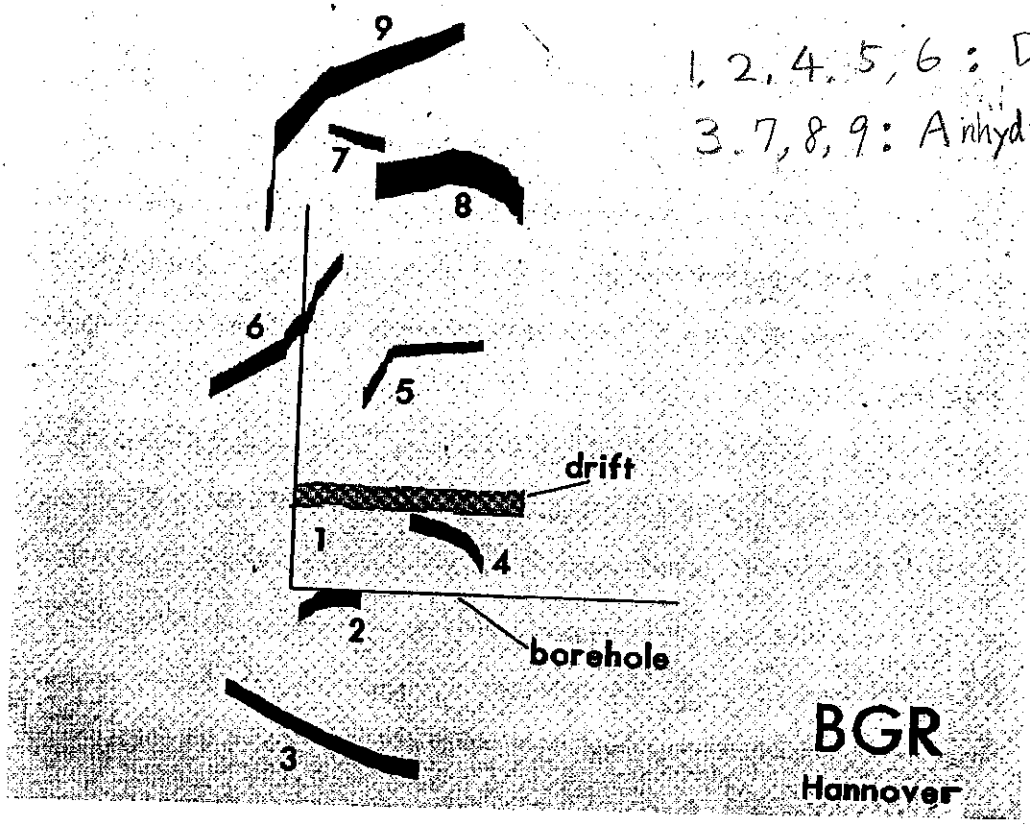

1, 2, 4, 5, 6 : Drifts
3, 7, 8, 9 : Anhydrite layer

Fig. 7: View from above.

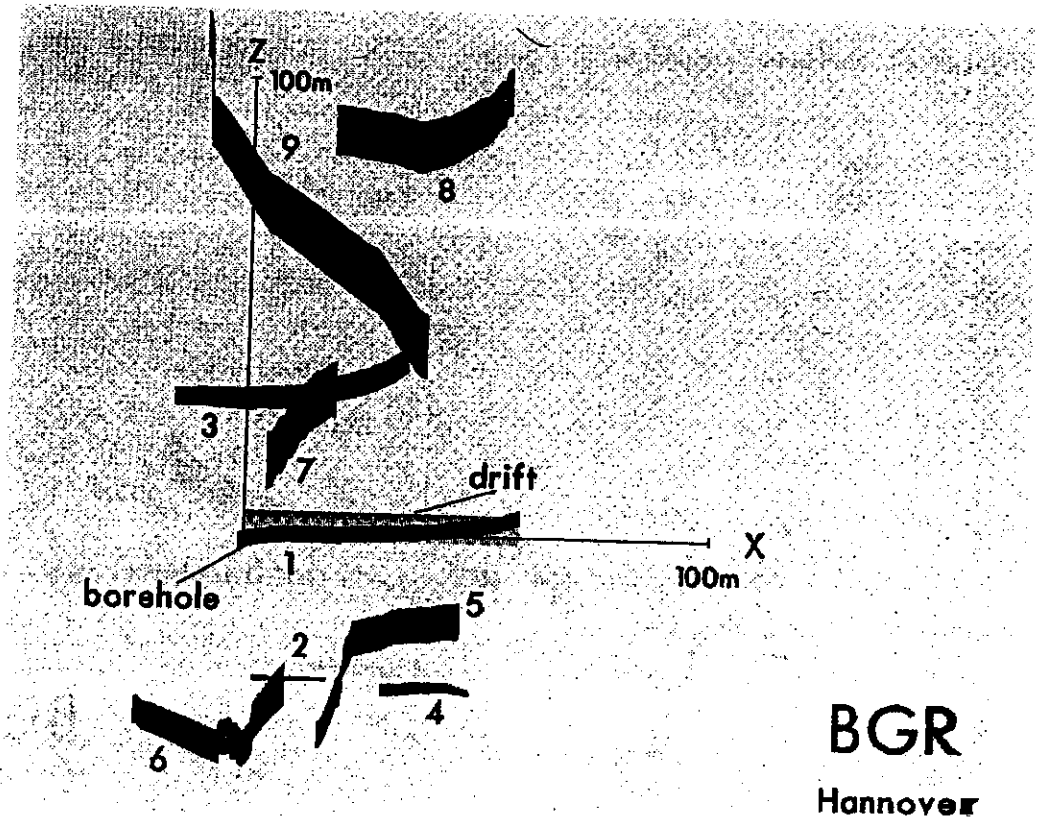

Fig. 8: View from the side.

Fig. 9c. View from the above and the side

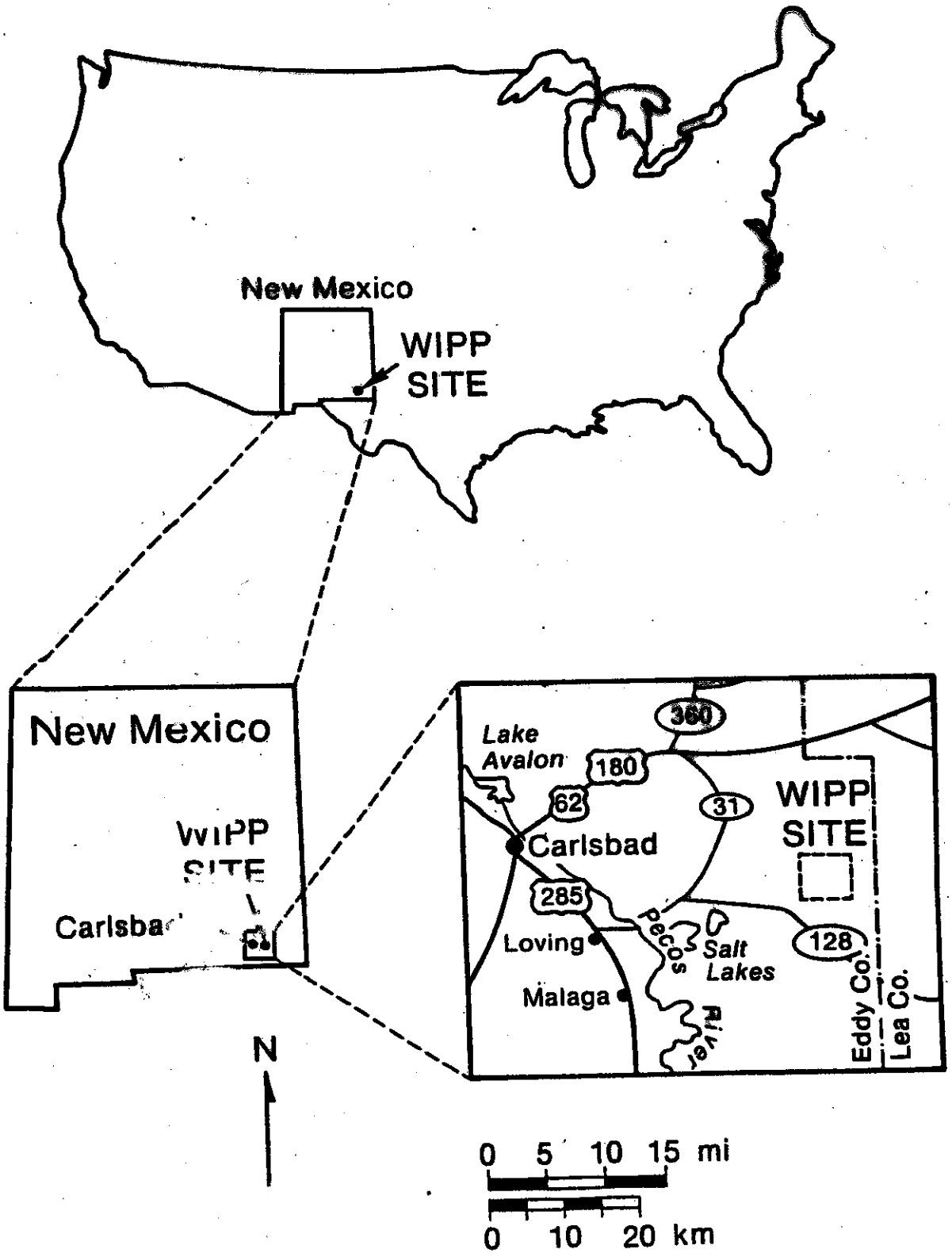

Fig. 10a.The Waste Isolation Pilot Plant, or WIPP, is the permanently dispose of transuranic radioactive waste left from the research etc in USA. It is located in the remote Chihuahuan Desert of Southeastern New Mexico,

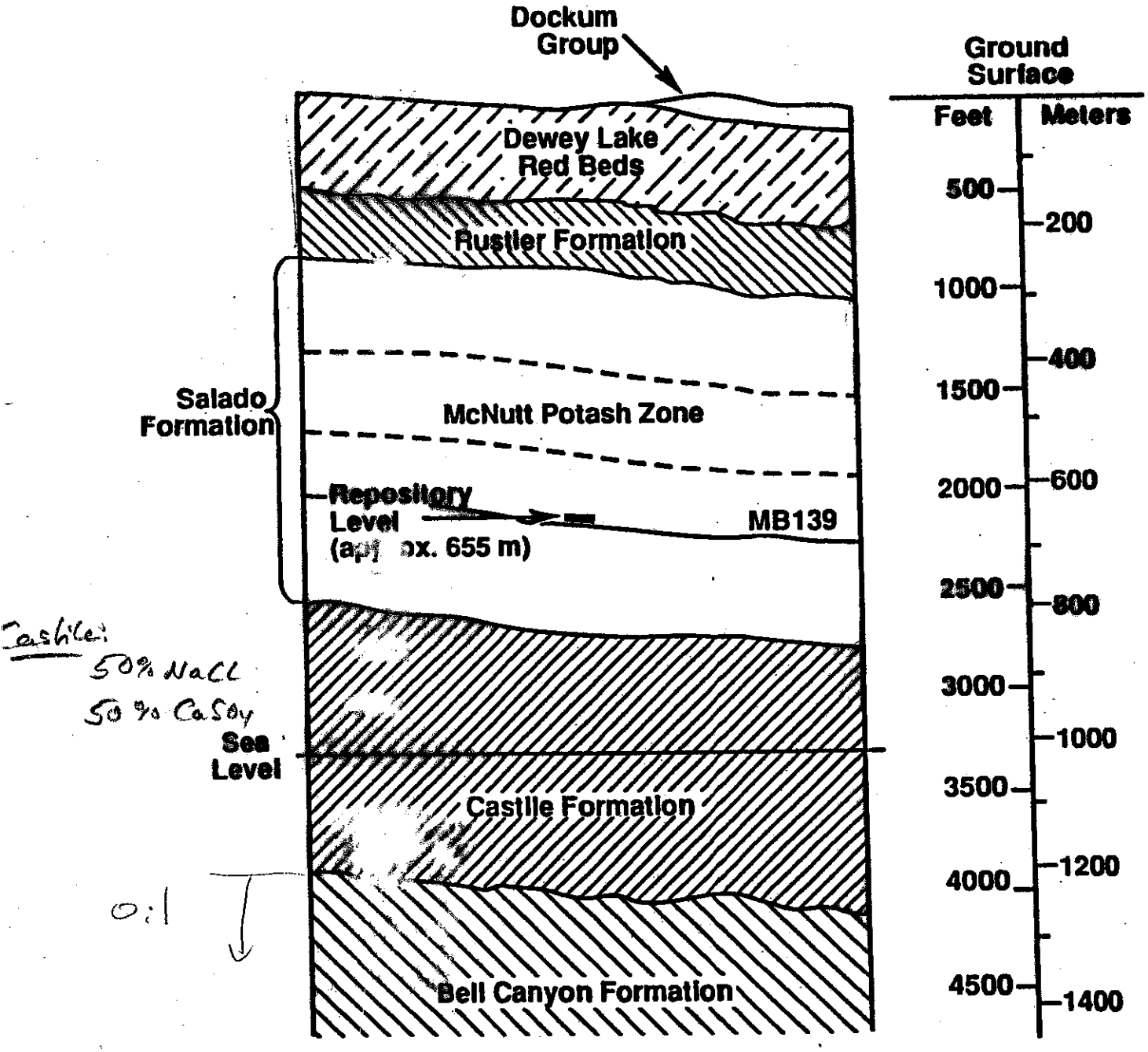

Generalized WIPP stratigraphy

Fig. 10b. Structure of WIPP stratums.

Fig.10c. Spacial view of WIPP surface & underground facilities.

Salt Neutrino Detector

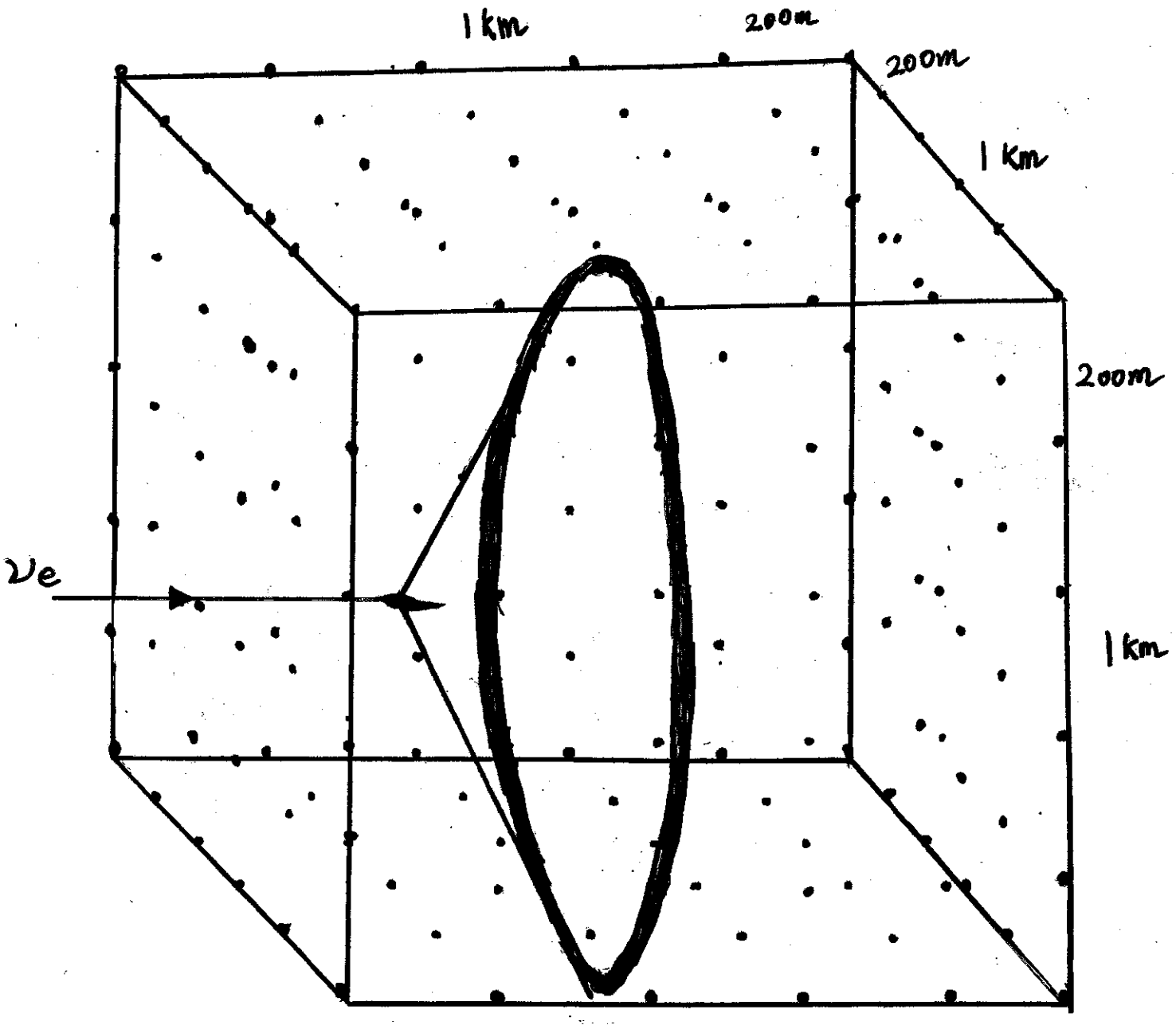

Fig. 11. Salt Neutrino Detector (SND) underground. Radio sensors of 216 are arrayed regularly in 200m repetition inside a 1km x 1km x 1km rock salt. Six radio sensors are hung on a string. The string is lowered in a well with the depth of over 1km. At the total 36 wells should be bored. A coherent Cherenkov radiation with the emission angle of 66 deg is generated by excess electrons in the shower in the UHE neutrino interaction.

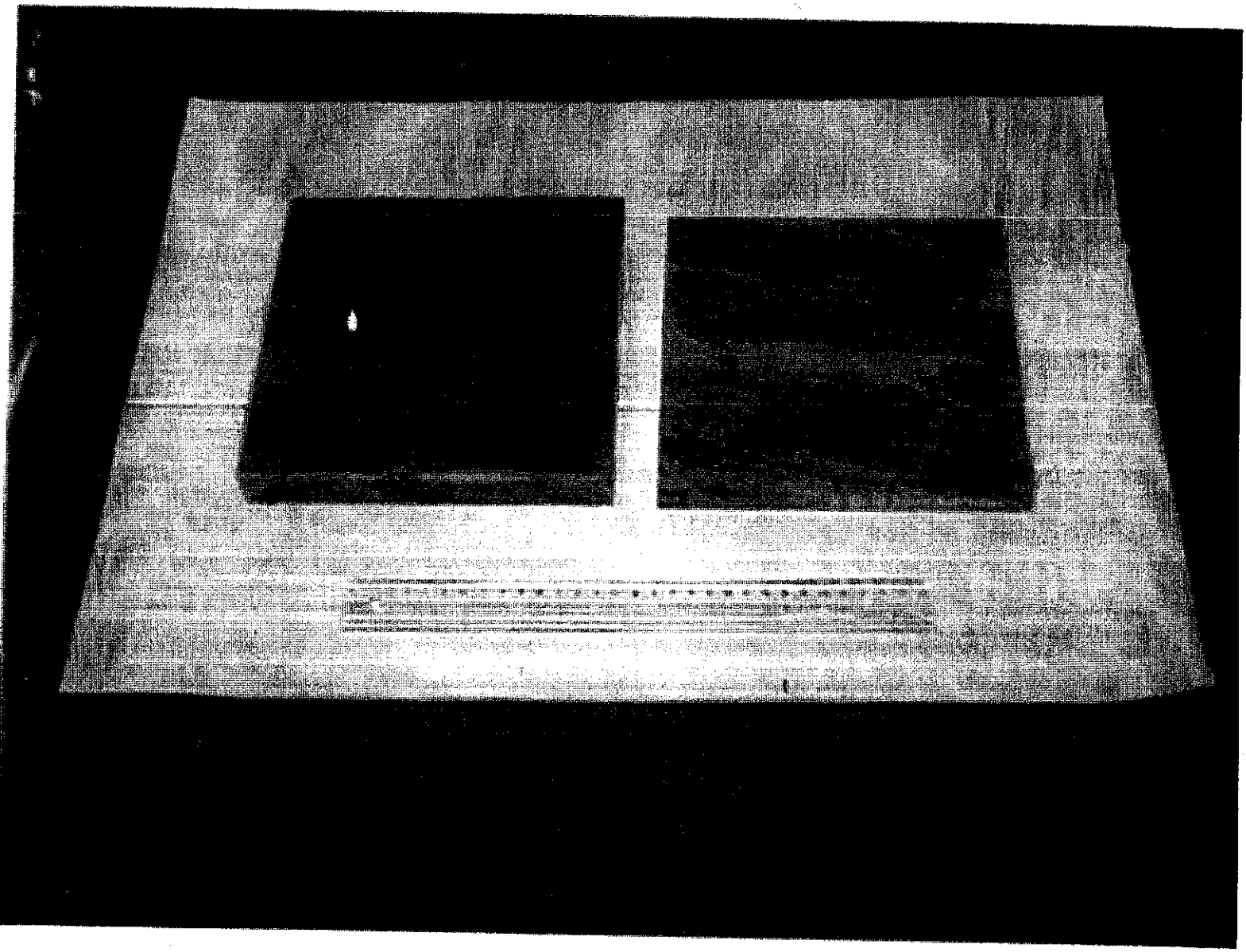

Hallstatt Salt Mine, Austria

Fig. 12a. Rock salt samples from Hallstadt salt mine [(1)200mm x 200mm x 11mm, (2)200mm x 200mm x 30mm], Austria.

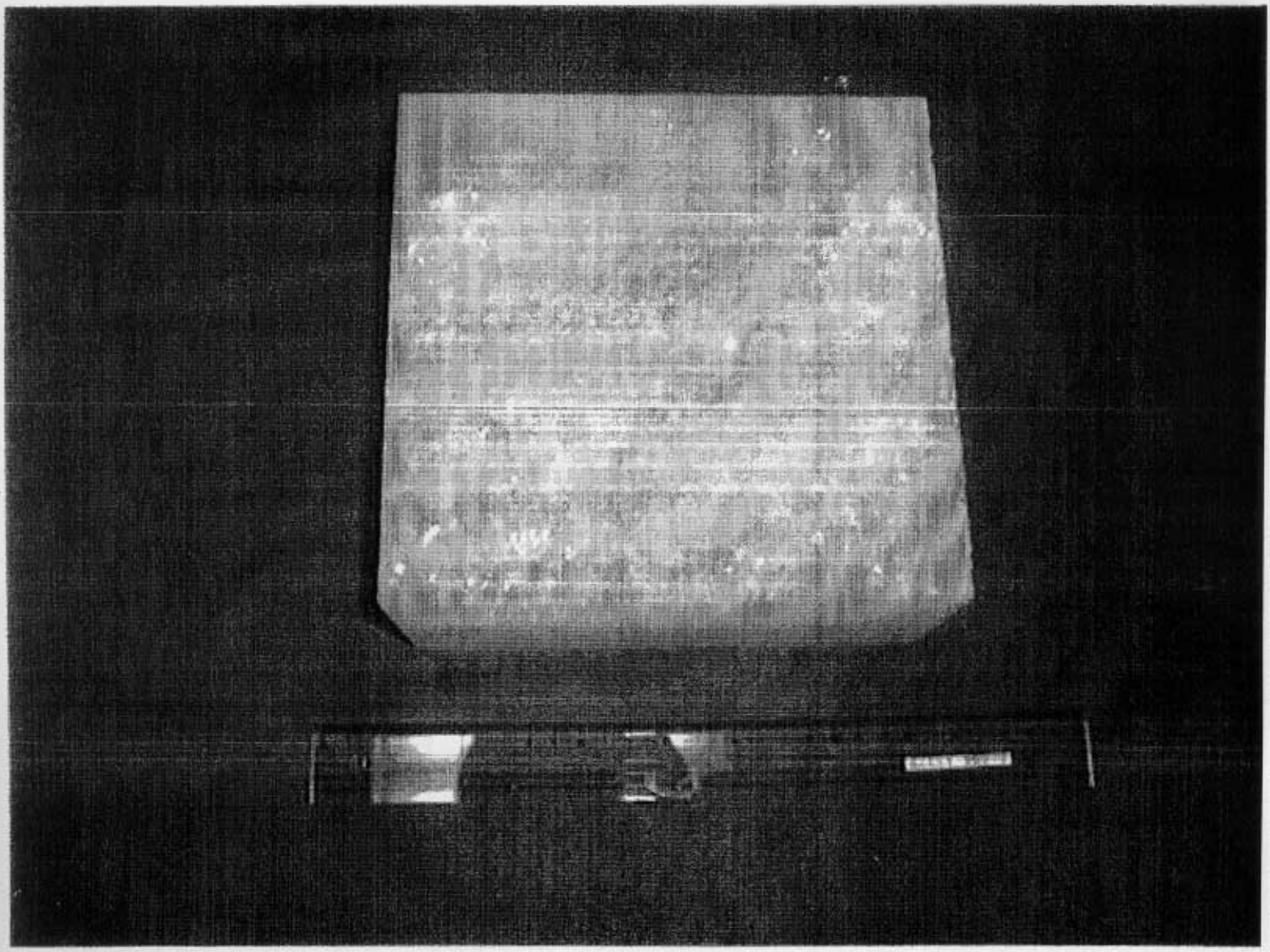

Asse Salt Mine, Germany

Fig. 12b. Rock salt samples from Asse salt mine [(3)200mm x 200mm x 99mm], Germany.

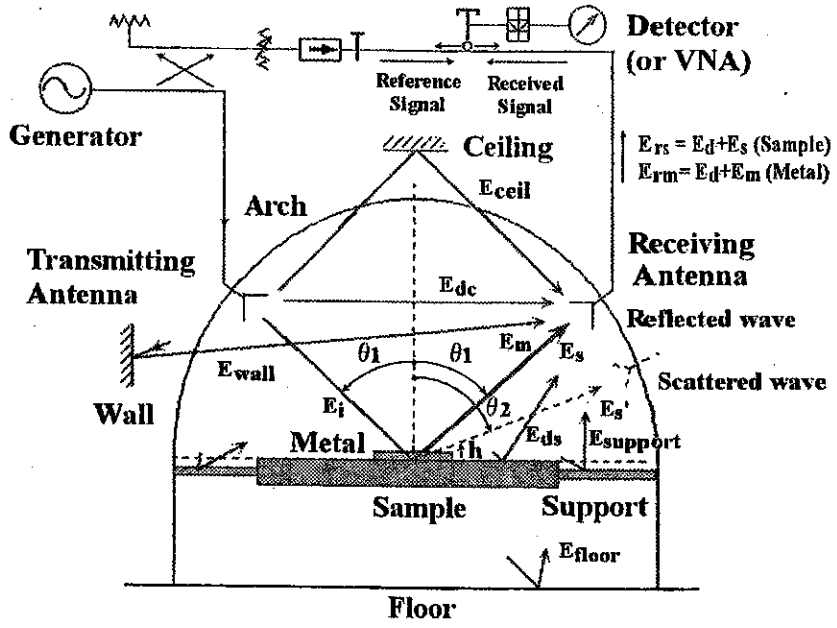

Fig. 4 Various direct-wave components in the non-destructive scattering-coefficient measurement method.

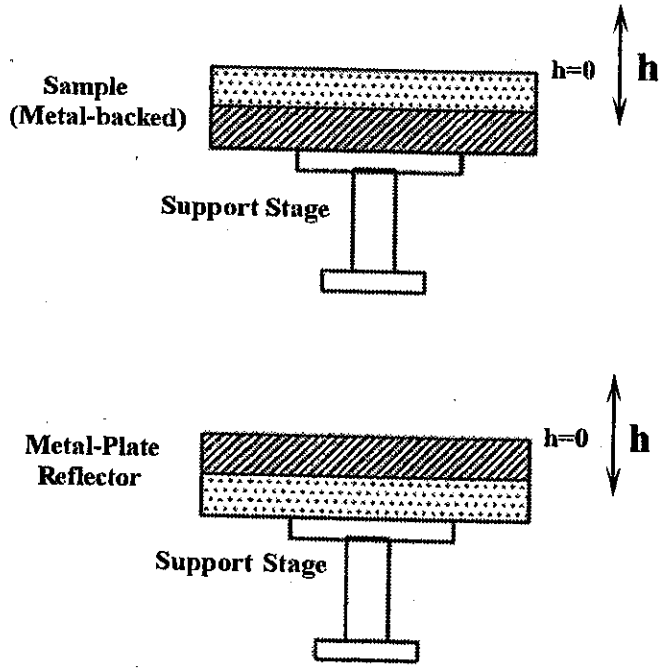

Fig. 6 Arrangement of sample and metal plates in the scattering-coefficient measurement method using a movable specimen.

Fig. 13a. Measurement of permittivity with a free space method at 9.4GHz in a non-destructive manner. The measurement was done by a vector network analyzer HP85107A. The microwave was radiated downward with the incident angle of 5 degree to a sample by a horn antenna having an aperture of 97mm x 68mm.

Fig. 13b. A photo of the measuring apparatus with a sample from Asse salt mine. [23]Ryouichi Ueno and Toshio Kamijo, IEICE Trans. Commun. E83B(2000)1554-1562; Ryouichi Ueno and Toshio Kamijo, Memoirs of Graduate School of Engineering, Tokyo Metropolitan University, No.48, 1998, pp5743-5752 (1999-02).

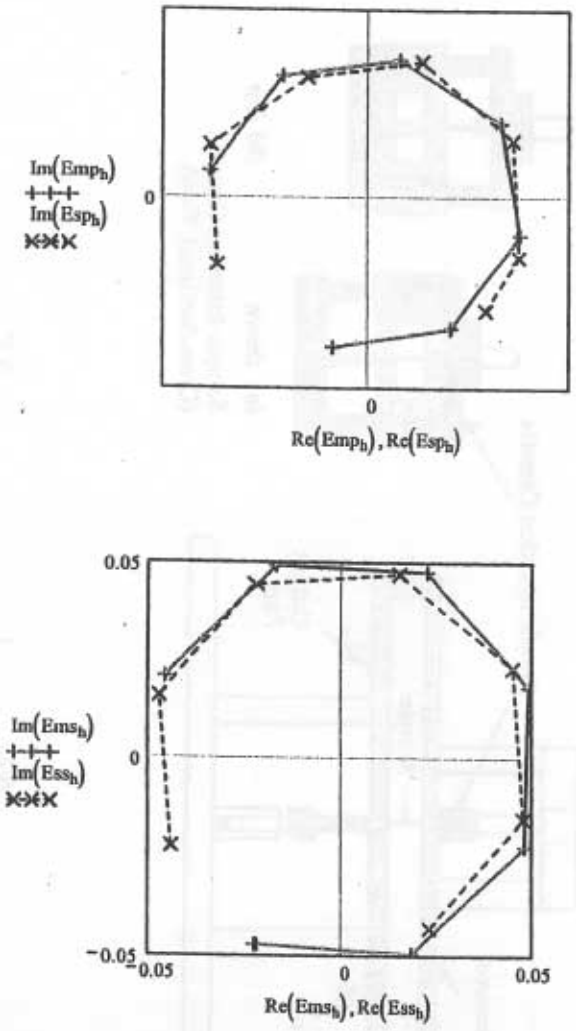

Fig. 14. The measurement was done at each position of the sample being separated in 2mm which corresponds to 50 deg. change in phase. The measured complex values of recieved signal are plotted in each position with (solid line) and without (dotted line) metal plate. The upper figure is in parallel and downward in perpendicular polarization with the scattering plane. Naively, in case of single reflection at the bottom surface of the sample, the angle and the radius differences in the complex plane correspond to real and imaginary permittivity, respectively. In more precise analysis, we take into account the multiple paths between the upper and the lower surfaces inside the sample.

TE_{10n} Rectangular Cavity Resonator at 9.4GHZ without insertion hall.

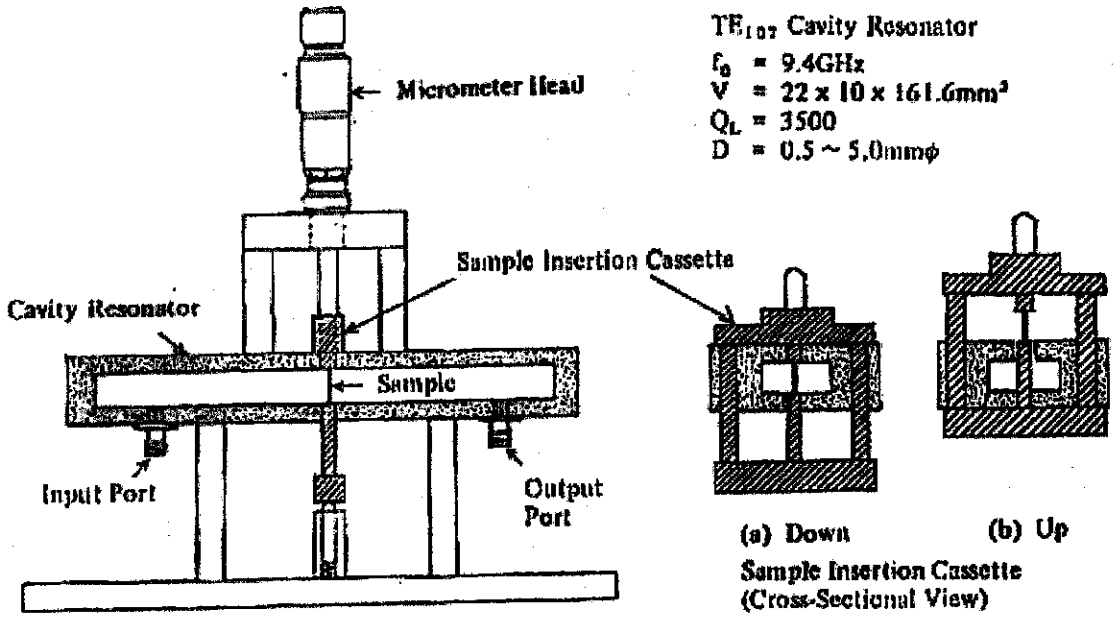

$$\frac{\Delta\lambda}{\lambda_0} \cdot j\frac{1}{2Q_s} = \alpha_s \cdot (\epsilon - 1) \cdot \frac{\Delta V}{V}$$

where 1/Qs is the loss factor of the sample, α_s is a constant determined by the mode of the resonator and the shape of the sample. α_s=2 and $\Delta V/V$ is the filling factor of the sample.

Fig. 15a . Permittivity measuring apparatus of a perturbed cavity resonator.

TE_{10n} Rectangular Cavity Resonator at 9.4GHZ without insertion hall.(Photograph)

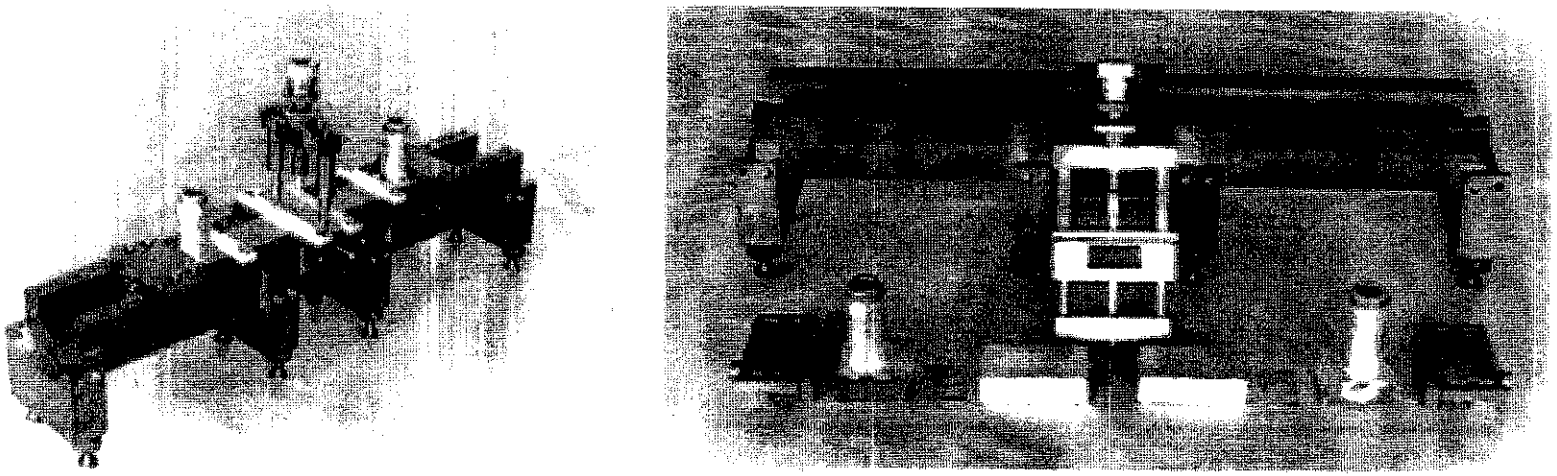

TM_{010} Cylindrical Cavity Resonator at 9.4GHZ without insertion hall.(Photograph)

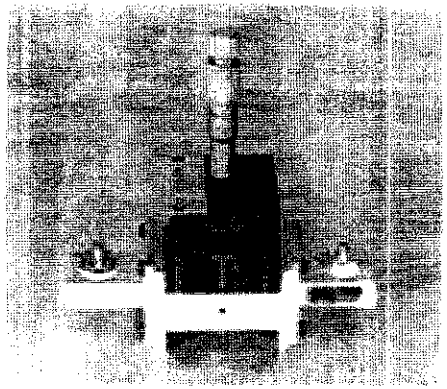

Fig. 15b. A photo of a perturbed cavity resonator.